DispatchDate: 22.09.2021 · ProofNo: 467, p.1

nature metabolism

ARTICLES

https://doi.org/10.1038/s42255-021-00467-8

Small extracellular vesicle-mediated targeting of hypothalamic AMPKα1 corrects obesity through BAT activation

Edward Milbank[1,2,3], Nathalia R. V. Dragano[1,2], Ismael González-García[1,2,4], Marcos Rios Garcia[1,2], Verónica Rivas-Limeres[1,2], Liliana Perdomo[3], Grégory Hilairet[3], Francisco Ruiz-Pino[2,5], Patricia Mallegol[3], Donald A. Morgan[6], Ramón Iglesias-Rey[7], Cristina Contreras[1,2], Luisa Vergori[3], Juan Cuñarro[1,2], Begoña Porteiro[1,2], Aleix Gavaldà-Navarro[8], Rebecca Oelkrug[9], Anxo Vidal[1], Juan Roa[2,5], Tomás Sobrino[7], Francesc Villarroya[2,8], Carlos Diéguez[1,2], Rubén Nogueiras[1,2], Cristina García-Cáceres[4,10], Manuel Tena-Sempere[2,5,11], Jens Mittag[9], M. Carmen Martínez[3], Kamal Rahmouni[6], Ramaroson Andriantsitohaina[3] ✉ and Miguel López[1,2] ✉

Current pharmacological therapies for treating obesity are of limited efficacy. Genetic ablation or loss of function of AMP-activated protein kinase alpha 1 (AMPKα1) in steroidogenic factor 1 (SF1) neurons of the ventromedial nucleus of the hypothalamus (VMH) induces feeding-independent resistance to obesity due to sympathetic activation of brown adipose tissue (BAT) thermogenesis. Here, we show that body weight of obese mice can be reduced by intravenous injection of small extracellular vesicles (sEVs) delivering a plasmid encoding an AMPKα1 dominant negative mutant (AMPKα1-DN) targeted to VMH-SF1 neurons. The beneficial effect of SF1-AMPKα1-DN loaded sEVs is feeding-independent and involves sympathetic nerve activation and increased BAT UCP1-dependent thermogenesis in BAT. Our results underscore the potential of sEVs to specifically target AMPK in hypothalamic neurons and introduce a broader strategy to manipulate body weight and reduce obesity.

Obesity causes thousands of deaths per year worldwide. This is due to the many direct and indirect comorbidities associated with this condition including cancer, cardiovascular diseases and type 2 diabetes (T2D) and yet it is the most preventable epidemic[1–6]. The most effective treatment of obesity is bariatric surgery, which not only decreases body weight but also improves T2D. However, most obese participants do not qualify for bariatric surgery. In addition, given the harmful and risky side effects of bariatric surgery, growing efforts are made to develop innovative antiobesity drugs[1,2,5]. However, even if some current pharmacological-driven strategies exhibit some beneficial outcomes in decreasing body weight, most of them display undesired side effects, mainly due to lack of specificity. Moreover, most of the current strategies are designed to target the food intake component of energy balance, while not many of them trigger energy expenditure. Indeed, as the regulation of body weight is complex and interconnected to multiple organism functions, increasing the specificity of the treatments by the identification of new molecular targets appears to be crucial[1,2,5].

AMPK is a cellular gauge that is activated in conditions of low energy, promoting counterregulatory responses[3,7–11]. Recent evidence has demonstrated that modulation of AMPK in the hypothalamus is a canonical mechanism regulating energy balance. In particular, hormonal, pharmacological or genetic inhibition of AMPKα1 in the VMH leads to an increase in sympathetic nervous system (SNS) activity, which stimulates BAT thermogenesis, elevating energy expenditure and subsequently leading to feeding-independent weight loss[12–18]. At a cellular level, this action occurs in SF1 neurons of the VMH, in which the specific deletion of AMPKα1 promotes resistance to diet-induced obesity (DIO) and metabolic improvement in mice[17,18].

The aim of this study is to develop a new strategy for the treatment of obesity by specifically targeting hypothalamic AMPKα1 in SF1 neurons. For this, we used sEVs[19–22], as carriers of plasmids encoding a dominant negative AMPKα1 mutant (AMPKα1-DN), which was previously validated by our group using virogenetic approaches[12–18,23]. sEVs are derived from multivesicular bodies and

[1]Department of Physiology, CiMUS, University of Santiago de Compostela-Instituto de Investigación Sanitaria, Santiago de Compostela, Spain. [2]CIBER Fisiopatología de la Obesidad y Nutrición (CIBEROBN), Madrid, Spain. [3]SOPAM, U1063, INSERM, University of Angers, SFR ICAT, Bat IRIS-IBS, Angers, France. [4]Institute for Diabetes and Obesity, Helmholtz Diabetes Center, Helmholtz Zentrum München, German Research Center for Environmental Health (GmbH), German Center for Diabetes Research (DZD), Neuherberg, Germany. [5]Department of Cell Biology, Physiology and Immunology, University of Córdoba; Instituto Maimónides de Investigación Biomédica (IMIBIC)/Hospital Universitario Reina Sofía, Córdoba, Spain. [6]Department of Neuroscience & Pharmacology, University of Iowa Carver College of Medicine, Iowa City, IA, USA. [7]Clinical Neurosciences Research Laboratory, Instituto de Investigación Sanitaria, Santiago de Compostela, Spain. [8]Institut de Biomedicina de la Universitat de Barcelona—Institut de Recerca Hospital Sant Joan de Déu, IBUB-IRSJD, Barcelona, Spain. [9]Institute for Endocrinology and Diabetes—Molecular Endocrinology, Center of Brain Behavior and Metabolism CBBM, University of Lübeck, Lübeck, Germany. [10]Medizinische Klinik and Poliklinik IV, Klinikum der Universität, Ludwig-Maximilians-Universität München, Munich, Germany. [11]FiDiPro Program, Institute of Biomedicine, University of Turku, Turku, Finland. ✉e-mail: ramaroson.andriantsitohaina@inserm.fr; m.lopez@usc.es

contain proteins, lipids and genetic information able to modify the phenotype and function of the target cells, which enables them to play a crucial role in physiology and pathophysiology[19–22]. Because of this broad spectrum of putative activities, sEVs can be exploited for prognosis, biomarkers and innovative therapy[19–22,24–26]. To confer specificity to the expression of this AMPKα1-DN mutant, the SF1 promoter was used to drive its expression. Notably, to avoid any invasive cranial surgery/procedure, the objective of this study was to target specifically AMPKα1 within hypothalamic SF1 neurons using systemic administration routes, namely intravenous injections, and making them affordable for potential therapeutic use.

Results

Generation and characterization of neuronal-targeted sEVs. As required for any delivery organic system, immunologically inert vesicles had to be designed to limit the host immune reaction[27,28]. Immature dendritic cells were used to generate large quantities of sEVs harbouring low expression of T-cell activators such as major histocompatibility complex II (MHC-II), as well as clusters of differentiation 80 and 86 (CD80 and CD86)[27,28]. To confer neuronal targeting capacities to the produced sEVs, immature dendritic cells were genetically modified to transiently express a fusion protein composed of (1) lysosome-associated membrane protein 2b (Lamp2b), a protein highly expressed in sEV membranes[29], fused to (2) a specific glycoprotein derived from the neurotrophic rabies virus (RVG) that enables the blood–brain barrier (BBB) crossing through its binding to the nicotinic acetylcholine receptor (nAChR)[28,30]. Three days after the transfection with the Lamp2b-RVG plasmid, the sEVs were isolated, purified and analysed. The neuronal-targeted Lamp2b-RVG sEVs displayed higher levels of expression of Lamp2b compared to the native ones (Extended Data Fig. 1a,b) suggesting a good integration of Lamp2b-RVG at the sEV membrane. It was demonstrated that using this strategy, RVG was localized at the outer membrane of the sEVs without affecting their physical properties[28]. In agreement with the literature, the Lamp2b-RVG sEVs had a size distribution between 30 and 150 nm as determined by nanoparticle tracking analysis (NTA) (camera level 9, shutter 607 and gain 15, Fig. 1a). These results were confirmed by electron microscopy analysis (Fig. 1b). The size of the sEVs obtained by the two different methods (NTA and electron microscopy) is slightly different. This size difference is explained by the fact that the procedure to stain the sEVs for the electron microscopy induce their dehydration, lowering their size[31]. The sEVs expressed specific markers such as ALIX, TSG101, CD9 and CD81 (Fig. 1c), and lacked GRP94, a marker commonly used to evaluate extracellular vesicle purity (Extended Data Fig. 1c).

The capacity of the sEVs to efficiently deliver nucleic acids was evaluated in vitro using fluorescent nucleic probes, a small-interfering RNA labelled with Texas Red and a green fluorescent protein (GFP) encoding plasmid. Once the sEVs were exogenously loaded with the nucleic acids, they were incubated with immature dendritic cells during 2, 6 or 24 h and the respective cell fluorescence was analysed using confocal microscopy. The siRNA-Texas Red-loaded sEVs induced red fluorescence of the immature dendritic cells after 2 h compared to the control conditions (non-loaded sEVs, Fig. 1d). In the same way, GFP plasmid-loaded sEVs induced green fluorescence of the immature dendritic target cells after 6 and 24 h compared to the control condition (Fig. 1e). We next evaluated the ability of the Lamp2b-RVG sEVs to cross the BBB following an intravenous injection. The sEVs were labelled with a near-infrared dye, DID (1,1′-dioctadecyl-3,3,3′,3′-tetramethylindodicarbocyanine,4-chlorobenzenesulfonate salt), which emits fluorescence when incorporated in lipid structures. To avoid any non-specific residual fluorescence of the DID, the labelled sEVs were washed twice before being injected. DID-labelled native (control) and DID-labelled Lamp2b-RVG sEVs were subsequently injected in the tail vein of nude mice. Anaesthetized live mice were imaged using DID-fluorescence spectra (excitation maximum 644 nm, emission maximum 665 nm) at 30 min, 2, 4 and 6 h using the in vivo fluorescence imaging system MAESTRO. The level of resolution from fluorescent whole mouse imaging (Fig. 1f) did not allow us to determine accurately from which tissue the DID-fluorescent signal originated. Thus, the animals were euthanized at 6 h, the different organs collected and the fluorescence analysed ex vivo. The two populations of sEVs, native (control) and Lamp2b-RVG, mostly distributed to the lungs, the spleen and the liver, with a lower lung targeting for the Lamp2b-RVG population compared to the control one (Fig. 1g). This distribution profile being consistent as these organs are highly vascularized and implicated in detoxification processes. The Lamp2b-RVG sEVs displayed a significantly increased localization in nAChR expressing tissues, such as the heart (Fig. 1g) and brain (Fig. 1h,i) compared to the native sEVs control condition. The percentage of uptake by the brain in relation to the total fluorescence was $2.3 \pm 0.3\%$; when fluorescence was corrected by tissue weight, the percentage of uptake ascended to $5.3 \pm 0.7\%$ fluorescence per mg. Moreover, the DID-specific fluorescence in the brain was significantly increased using the Lamp2b-RVG targeting strategy (control, 100 ± 5.01; Lamp2b-RVG, 129 ± 0.65; $P < 0.01$; Fig. 1h,i), confirming its suitability to increase the targeting of the sEVs to the central nervous system (CNS)[28].

Once we had demonstrated that the sEVs could reach the brain, the next step was to limit the specificity of the delivery to the exclusive VMH and specifically to the SF1 cells, which is the unique cell population expressing this factor in the CNS[32,33]. For this, we designed a plasmid encoding an AMPKα1-DN mutant expressed under the control of SF1 promoter (SF1-AMPKα1-DN) (Extended Data Fig. 1d). The purified neuronal-targeted Lamp2b-RVG sEVs were subsequently loaded with SF1-AMPKα1-DN. The loading did not modify either the size or the morphological properties of the sEVs as measured by NTA at camera level 9 (shutter, 607 and gain, 15) and electron microscopy (Fig. 1a and Extended Data Fig. 1e,f). Moreover, the amount of encapsulated SF1-AMPKα1-DN plasmid was assayed with or without lysis of the sEVs with Triton X-100 0.2% (Extended Data Fig. 1g,h) indicating the presence of the SF1-AMPKα1-DN plasmid at the membrane and inside the sEV core.

Then, we evaluated the efficacy of this strategy by assaying the phosphorylated levels of acetyl-CoA carboxylase alpha (pACCα), a main downstream target of AMPK, in the hypothalamic cell line GT1-7, which endogenously express SF1 (ref. [34]) and possess a number of neuronal characteristics[35] making them an excellent model for preliminary AMPK neuronal studies[36,37]. The data showed that the levels of phosphorylation of ACCα were significantly decreased when GT1-7 cells were incubated for 24 h with SF1-AMPKα1-DN loaded sEVs, compared to non-loaded control sEVs (Fig. 1j,k). Notably, when other CNS-derived cells not expressing SF1, such as primary astrocytes and Neuro2A cells, were incubated with SF1-AMPKα1-DN loaded sEVs, no changes were found in pACC levels (Extended Data Fig. 1i,j). Altogether, these data indicate that the generated Lamp2b-RVG sEVs loaded with SF1-AMPKα1-DN mutants are (1) homogenous in size and morphology and are able to (2) deliver nucleic acids, (3) target the brain following an intravenous injection and (4) specifically regulate AMPKα1 activity under the control of SF1 promoter in vitro.

Central SF1-AMPKα1-DN sEVs induce weight loss. First, we assessed the efficacy of stereotaxic central delivery of SF1-AMPKα1-DN loaded sEVs in the VMH of DIO mice that were fed with a 60% high-fat diet (HFD). The results demonstrated that when administrated within this nucleus, SF1-AMPKα1-DN sEVs induced a feeding-independent weight loss for 3 d (Fig. 2a,b). Next,

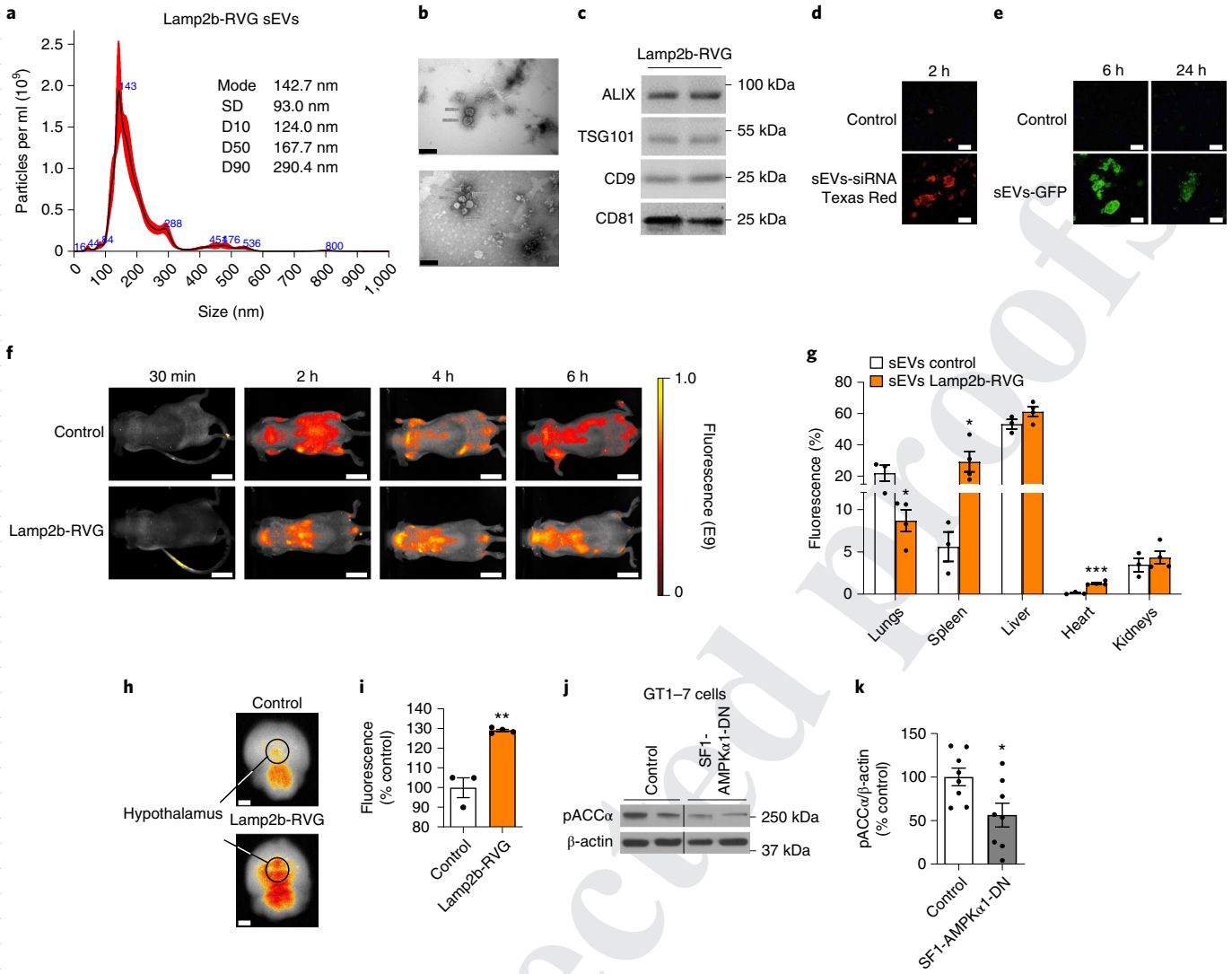

Fig. 1 | Generation and characterization of neuronal-targeted dendritic cell-derived sEVs. a, Example of a curve obtained by NTA of a sample of Lamp2b-RVG sEVs. The graph represents concentration of sEVs (particles per ml) according to the size (nm). **b**, Electron microscopy image of generated Lamp2b-RVG sEVs; scale bars represent 100 nm. The experiments were repeated three times. **c**, Western blotting using antibodies against ALIX, TSG101, CD9 and CD81 in Lamp2b-RVG sEVs. The experiments were repeated twice. **d**,**e**, Confocal microscopy images of JAWS II cells treated with non-loaded sEVs (control), siRNA-Texas Red-loaded sEVs (sEVs-siRNA-Texas Red) or GFP plasmid-loaded sEVs (sEVs-GFP) at 2 h (**d**) and 6 and 24 h (**e**). Scale bars represent 20 µm; control $n=1$ field; sEVs-siRNA-Texas Red and sEVs-GFP $n=3$ fields. **f**, Representative MAESTRO images at 30 min, 2, 4 and 6 h of live mice injection intravenously with DID-labelled native (control) or DID-labelled Lamp2b-RVG sEVs (Lamp2b-RVG); scale bars represent 2 cm. The analysis was repeated three (control) and four times (Lamp2b-RVG sEVs). **g**, Ex vivo quantification of DID fluorescence on isolated organs (lungs, spleen, liver, heart and kidneys) 6 h postinjection with DID-labelled native (control, $n=3$) or DID-labelled Lamp2b-RVG sEVs (Lamp2b-RVG, $n=4$); lungs $P=0.031$, spleen $P=0.029$, heart $P=0.00048$. **h**, Representative images of mouse brains, black circles delimit hypothalamus, collected 6 h postinjection of DID-labelled native (control, $n=3$ mice) and DID-labelled Lamp2b-RVG sEVs (Lamp2b-RVG, $n=4$ mice); scale bars represent 2 mm. The analysis was repeated three (control) and four times (Lamp2b-RVG sEVs). **i**, Ex vivo quantification of DID fluorescence of mouse brains collected 6 h postinjection of DID-labelled native (control, $n=3$ mice) and DID-labelled Lamp2b-RVG sEVs ($n=4$ mice). **j**, Representative pACCα western blot images of GT1-7 cells treated for 24 h with control (non-loaded) or SF1-AMPKα1-DN loaded sEVs; $P=0.0010$. ß-actin was used as control of protein loading. A black line was inserted on the immunoblots when samples were loaded on the same gel, but not side by side. **k**, Quantification of pACCα in GT1-7 cells treated for 24 h with control (non-loaded) or SF1-AMPKα1-DN loaded sEVs ($n=8$ samples per group); $P=0.0219$. Data are expressed as mean ± s.e.m. $^*P<0.05$, $^{**}P<0.01$ and $^{***}P<0.001$ versus controls. Statistical significance was assessed by a two-sided Student's *t*-test.

we assayed the levels of pACCα (a surrogate marker of AMPK activity) in microdissected hypothalamic extracts, as previously shown[15–17]. Specificity of the micropunches was routinely validated by measuring the messenger RNA levels of Sf1 (specific marker of the VMH), proopiomelanocortin (Pomc, a specific marker of the arcuate nucleus of the hypothalamus (ARC)) and hypocretin/orexin (a specific marker of the lateral hypothalamic area (LHA)), respectively (Extended Data Fig. 2). Our data showed that SF1-AMPKα1-DN loaded sEVs induced a significant decrease in the phosphorylated levels of ACCα in the VMH, but not in the ARC or the LHA (Fig. 2c,d). This was associated with increased BAT thermogenesis as indicated by the elevated temperature in the interscapular area and enhanced BAT uncoupling protein 1 (UCP1) protein levels (Fig. 2e–h). Overall, these data recapitulate the effects

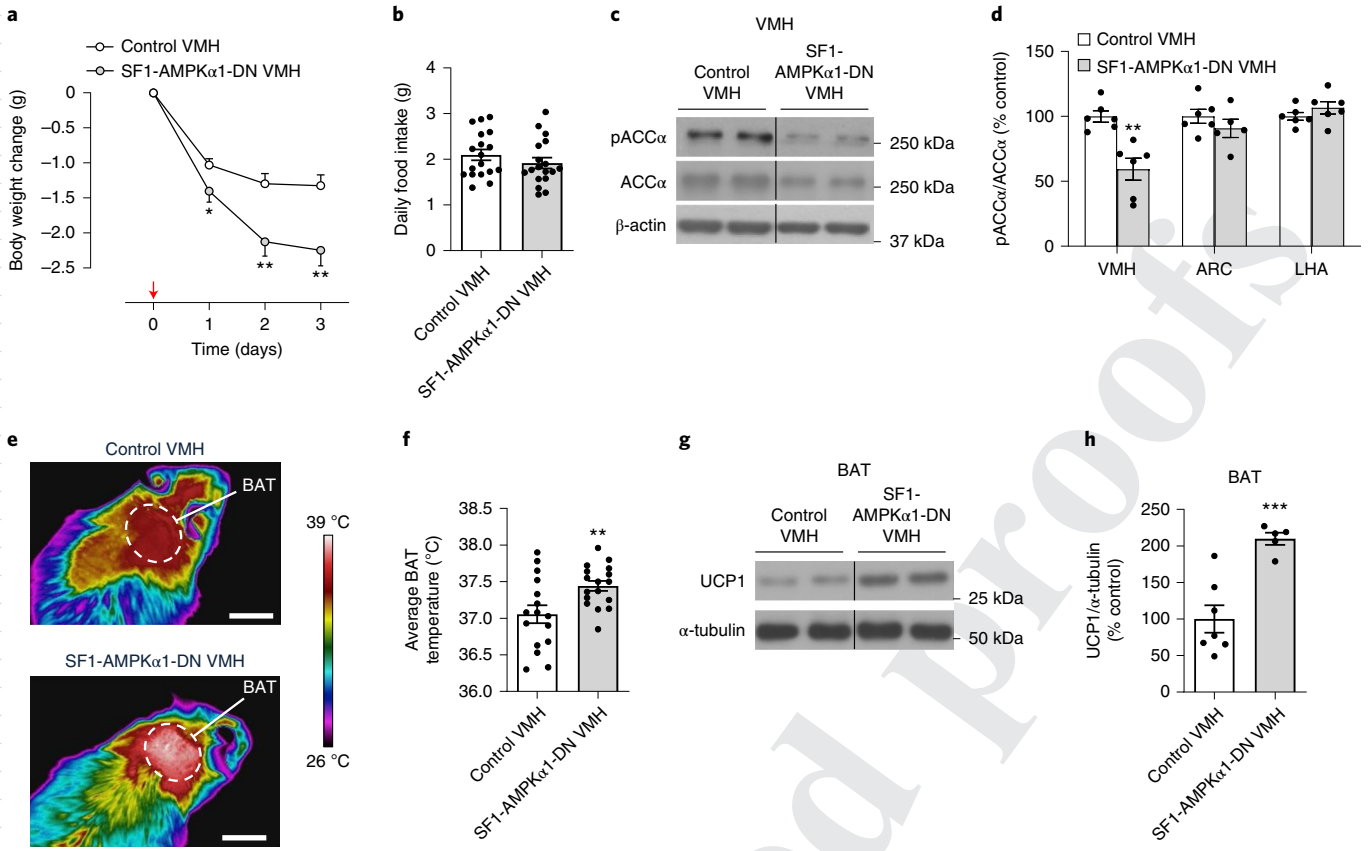

Fig. 2 | Effect of stereotaxic VMH injection of SF1-AMPKα1-DN loaded sEVs on energy balance in DIO mice. a, Body weight changes of mice after stereotaxic VMH injection with control (non-loaded, $n=18$ mice) or SF1-AMPKα1-DN loaded sEVs ($n=19$ mice). The red arrow indicates the onset of injections; day 1 $P=0.048$; day 2 $P=0.002$ and day 3 $P=0.0017$. **b**, Daily food intake of mice after stereotaxic VMH injection with control (non-loaded) or SF1-AMPKα1-DN loaded sEVs ($n=18$ mice per group). **c**, Representative pACCα and ACCα western blot images in VMH collected from mice after 72 h of stereotaxic VMH injection with control (non-loaded) or SF1-AMPKα1-DN loaded sEVs. β-actin was used as control of protein loading. A black line was inserted on the immunoblots when samples were loaded on the same gel, but not side by side. The experiment was performed twice. **d**, Quantification of pACCα/ACCα in VMH ($n=6$ mice per group, $P=0.0015$), ARC (control $n=6$ mice, SF1-AMPKα1-DN $n=5$ mice) and LHA ($n=6$ mice per group). **e**,**f**, Representative thermographic images, scale bars represent 1 cm (**e**) and BAT interscapular temperature quantification (average of the 3 days) (**f**) of mice after 72 h of stereotaxic VMH injection with control (non-loaded, $n=16$ mice) or SF1-AMPKα1-DN loaded sEVs ($n=17$ mice); $P=0.0090$. **g**, Representative UCP1 western blot images of BAT collected from mice after 72 h of stereotaxic VMH injection with control (non-loaded) or SF1-AMPKα1-DN loaded sEVs. α-tubulin was used as control of protein loading. A black line was inserted on the immunoblots when samples were loaded on the same gel, but not side by side. The experiment was performed twice. **h**, Quantification of UCP1 protein expression of BAT collected from mice after 72 h of stereotaxic VMH injection with control (non-loaded, $n=7$ mice) or SF1-AMPKα1-DN loaded sEV ($n=5$ mice); $P=0.0009$. Data are expressed as mean ± s.e.m. $^{**}P<0.01$ and $^{***}P<0.001$ versus control. Statistical significance was assessed by a two-sided Student's *t*-test.

of virogenetic-mediated treatment with AMPKα1-DN isoforms, as well as the phenotype of SF1-AMPK null mice[12–18].

Systemic SF1-AMPKα1-DN sEVs modulate hypothalamic AMPK. Next, we aimed to investigate the ability of systemic administration of SF1-AMPKα1-DN loaded sEVs in modulating AMPK activity in the hypothalamus of DIO mice. First, we evaluated the efficiency of our treatment by assaying the expression of the SF1-AMPKα1-DN transgene in several tissues 24 h after an intravenous injection of the loaded sEVs. The transgene was only detected in VMH samples, but not in any of the other evaluated organs including those expressing SF1 (that is, adrenal, pituitary and testis), or those not expressing SF1 (that is, BAT, liver, skeletal muscle and heart) (Fig. 3a). Overall, these data indicated that the expression of AMPKα1-DN transgene is restricted to neuronal cells (given the RVG-dependent tropism[28,30]), including the SF1-expressing neurons of the VMH (given the SF1-driven expression), demonstrating that our strategy was specific. To confirm those results, we assayed the phosphorylation levels of ACCα in several tissues after intravenous injections. SF1-AMPKα1-DN loaded sEVs induced a significant decrease in the levels of phosphorylation of ACCα and AMPK activity in the VMH (Fig. 3b–d). In keeping with this, SF1-AMPKα1-DN sEVs treated mice showed a significantly reduced number of pACCα-Ser[79] positive neurons within the VMH compared to the controls, as demonstrated by the colocalization of pACCα and Neurotrace (Fig. 3e,f). We also assessed the presence of pACCα in non-neuronal cells through costaining of glial fibrillary acidic protein (GFAP, an astrocyte marker) and ionized calcium binding adaptor molecule 1 (Iba1, a microglia marker) in the VMH. However, our analysis did not detect any pACCα colocalization with GFAP or Iba1-expressing cells (Extended Data Fig. 3a,b). To gain more insight in the specificity of our treatment, we analysed the levels of pACCα-Ser[79] in SF1 neurons of the VMH through double immunofluorescence assays. Our data showed that pACC immunoreactivity was significantly decreased in the SF1 neurons of mice treated with SF1-AMPKα1-DN sEVs (Fig. 3g,h), when

compared to the negative controls, demonstrating the specificity of the technique (Extended Data Fig. 3c). Notably, pACCα levels were not decreased in neighbouring hypothalamic nuclei such as the ARC, the dorsomedial and the paraventricular (Extended Data Fig. 3d). Overall, this evidence demonstrates that the expression of the SF1-AMPKα1-DN transgene occurs in SF1 neurons within the VMH, but not in other hypothalamic cell populations.

To further confirm the specificity of our treatment with SF1-AMPKα1-DN loaded sEVs, we investigated the pACC levels in other parts of the CNS and peripheral tissues. No changes were found in the phosphorylation levels of ACCα in any other brain areas tested (for example, cortex, thalamus and cerebellum; Extended Data Fig. 4a) or in peripheral tissues such as liver, adrenal gland, testis, BAT, heart and skeletal muscle (Extended Data Fig. 4b). SF1-AMPKα1-DN loaded sEVs did not induce changes in pACCα level in primary brown adipocytes (Extended Data Fig. 4c). These data also indicate that the potential side effects on blunting AMPK signalling in other tissues, including those that express SF1, such as testis and adrenal gland, are probably negligible. However, the use of an assay that relied on total protein extracts in peripheral tissues, where SF1 cells are scarce (for example, confined to testicular Leydig cells)[32,33] may not be considered reliable. To overcome this limitation and further assess the possible impact of the treatment on testicular and adrenal function, we analysed the circulating levels of testosterone and corticosterone (CORT) as well as the mRNA expression of key steroidogenic enzymes in the testis and adrenal gland of mice treated with control and SF1-AMPKα1-DN loaded sEVs. The data showed that treatment with SF1-AMPKα1-DN loaded sEVs did not induce any significant change either in testosterone circulating levels (Extended Data Fig. 4d) or in the mRNA levels of several enzymes involved in testicular steroidogenesis, such as steroidogenic acute regulatory protein (STAR), cholesterol side-chain cleavage enzyme (P450ssc) and 17ß-hydroxysteroid dehydrogenase type 3 (17ß-HSD3) (Extended Data Fig. 4e). On the other hand, adrenal function was not affected by the treatment with SF1-AMPKα1-DN loaded sEVs as no changes in circulating CORT (Extended Data Fig. 4f) or in the mRNA adrenal levels of P450ssc or STAR (Extended Data Fig. 4g) were detected. Similarly, no changes were found either in the circulating levels of luteinizing hormone (Extended Data Fig. 4h) or in the mRNA levels of the luteinizing hormone beta subunit (Extended Data Fig. 4i), which pituitary production is known to be regulated by SF1 (ref. [38]).

Systemic SF1-AMPKα1-DN sEVs induce weight loss. To evaluate the efficiency of SF1-AMPKα1-DN loaded sEVs in modulating body weight, we used DIO mice. Notably, to avoid any procedure or surgery involving direct administration into the CNS, mice were injected systemically in the tail vein. First, we evaluated how long the SF1-AMPKα1-DN transgene was expressed in the VMH-SF1 neurons after peripheral treatment with loaded sEVs. Our data showed that AMPKα1-DN transgene can be detected in the VMH for 24 h (Fig. 3i,j). However, and keeping with the experiment involving only central administration (Fig. 2h), the increased BAT UCP1 expression can be detected up to 48 h following an intravenous injection (Extended Data Fig. 4j). For these reasons, we selected a strategy based on one injection every 3 days for 6 days. We found that after a 6-day treatment (injections at days 0 and 3), the intravenous injections of SF1-AMPKα1-DN loaded sEVs induced a significant and marked feeding-independent weight loss in DIO mice, when compared to control sEVs (Fig. 4a,d), concomitantly with increased energy expenditure (Fig. 4e). Analysis of covariance (ANCOVA) analysing both group and body weight effects as covariate confirmed the significant increase in energy expenditure (Fig. 4f). However, respiratory quotient and locomotor activity were not modified (Fig. 4g,h). Of note, sEV-induced weight loss was associated with decreased adiposity, as demonstrated by nuclear magnetic resonance (NMR) analysis (Fig. 4i–l).

Next, we investigated the long-term effect (4 weeks, administration every 3 days) of sEV treatment in DIO mice. The results showed that when compared to mice treated with control sEVs, which normally increased their body weight, SF1-AMPKα1-DN loaded sEVs injected DIO mice displayed a marked long-term reduction in their body weight (Fig. 4m–o) with no changes in food intake (Fig. 4p–q). Of note, the effect of sEVs was sustained when the treatment was withdrawn. Indeed, DIO mice treated with SF1-AMPKα1-DN loaded sEVs did not exhibit any catch up in their body weight up until 2 weeks after the injections were ceased (washout), when compared to mice treated with control sEVs (Fig. 4m,n). Overall, these data indicate that the body weight loss induced by SF1-AMPKα1-DN loaded sEVs is not transient and a washout period does not indicate a rebound effect enough to catch up the body weight of the control group. The weight-reducing action of sEVs was associated with a trend to decrease circulating leptin levels (Extended Data Fig. 5a) while no changes in growth/differentiation factor 15 were observed (GDF15, Extended Data Fig. 5b). Assessment of circulating inflammatory markers showed no changes in interleukin-6 (IL-6) levels (Extended Data Fig. 5c) and interferon gamma-induced protein 10 (IP-10) levels (Extended Data Fig. 5d), suggesting that sEVs administration did not induce systemic inflammatory reaction. We also evaluated the effect of SF1-AMPKα1-DN loaded sEVs on circulating metabolic parameters. Our data showed significant decreased non-esterified fatty acids (NEFAs) circulating levels in the loaded

Fig. 3 | Effect of systemic treatment with SF1-AMPKα1-DN loaded sEVs on hypothalamic AMPK activity in DIO mice. a, SF1-AMPKα1-DN plasmid in vivo expression at 24 h in mice injected intravenously with SF1-AMPKα1-DN loaded sEVs. Representative agarose gel electrophoresis using specific SF1-AMPKα1-DN and HPRT primers. +Control is the SF1-AMPKα1-DN plasmid. The data originate from one single experiment. **b**, Representative pACCα and ACCα western blot images in the VMH after 72 h of intravenous injection with control (non-loaded) or SF1-AMPKα1-DN loaded sEVs ($n=6$ mice per group). β-actin was used as control of protein loading. A black line was inserted on the immunoblots when samples were loaded on the same gel, but not side by side. **c**, Quantification of pACCα/ACCα in VMH; $n=6$ mice per group, $P=0.044$. **d**, Quantification of AMPK activity in the VMH after 72 h of intravenous injection with control (non-loaded, $n=6$ mice) or SF1-AMPKα1-DN loaded sEVs ($n=5$ mice); $P=0.00097$. **e**,**f**, Representative confocal microscopy images depicting Neurotrace 500/525 (green), pACCα (magenta)-positive cells and merged reactivity (**e**) and quantification (**f**) of pACCα positive cell number (quantification per field; control $n=12$ fields, four mice per group; SF1-AMPKα1-DN $n=10$ fields, four mice per group) in the VMH after 24 h of intravenous injection with control (non-loaded) or SF1-AMPKα1-DN loaded sEVs. $P=0.00072$; scale bars represent 20 µm. **g**,**h**, Representative confocal microscopy images depicting DAPI (blue), SF1 (red), pACCα (green) and merged reactivity (**g**) and quantification of pACCα fluorescence (**h**) in SF1 cells (quantification per field; control $n=4$ fields, four mice per group; SF1-AMPKα1-DN $n=6$ fields, four mice per group) in the VMH after 24 h of intravenous injection with control (non-loaded) or SF1-AMPKα1-DN loaded sEVs; $P=0.0054$. Arrows indicate pACC-positive SF1 cells; scale bars represent 20 µm. **i**,**j**, Time course of SF1-AMPKα1-DN plasmid expression in the VMH following one intravenous injection. Representative agarose gel electrophoresis using specific SF1-AMPKα1-DN and HPRT primers (**i**) and quantification of SF1-AMPKα1-DN plasmid expression in the VMH (**j**) at different time points (days 0, 1, 3 and 7 $n=5$ mice per group; day 2 $n=2$ mice); days 0, 1, 3 and 7, $P=6.2172\times10^{-12}$; day 2, $P=3.05\times10^{-7}$. MWM, molecular weight marker. Data are expressed as mean ± s.e.m. $^{*}P<0.05$, $^{**}P<0.01$ and $^{***}P<0.001$ versus control. Statistical significance was assessed by a two-sided Student's *t*-test.

sEVs treated group, which would be compatible with the increased BAT thermogenesis (below), with no changes in total triglycerides or cholesterol (Extended Data Fig. 5e–g). Finally, to assess the possible adverse effects of our treatment, we analysed the impact of SF1-AMPKα1-DN loaded sEVs on aspartate transaminase (AST) and alanine transaminase (ALT), but none of them were altered

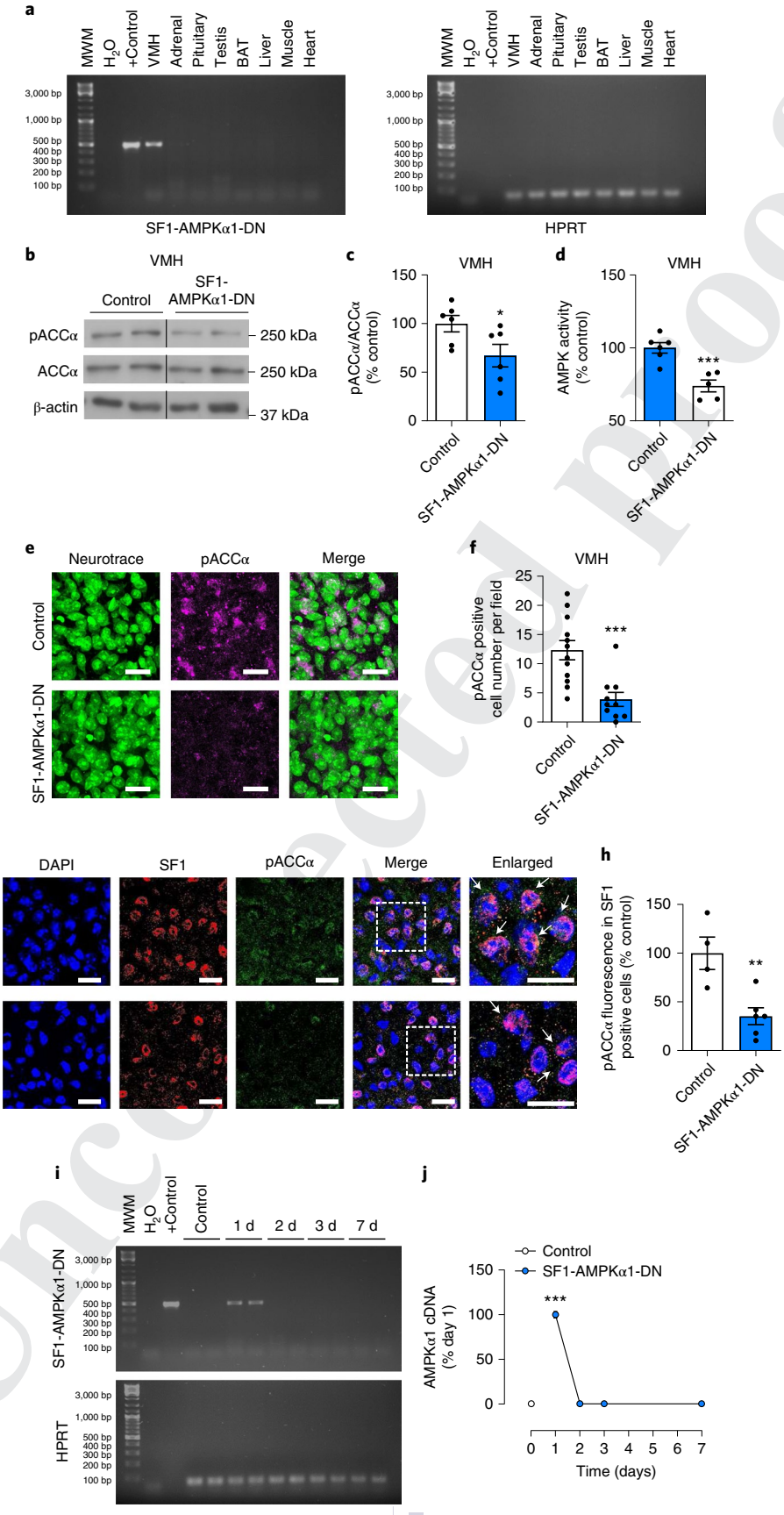

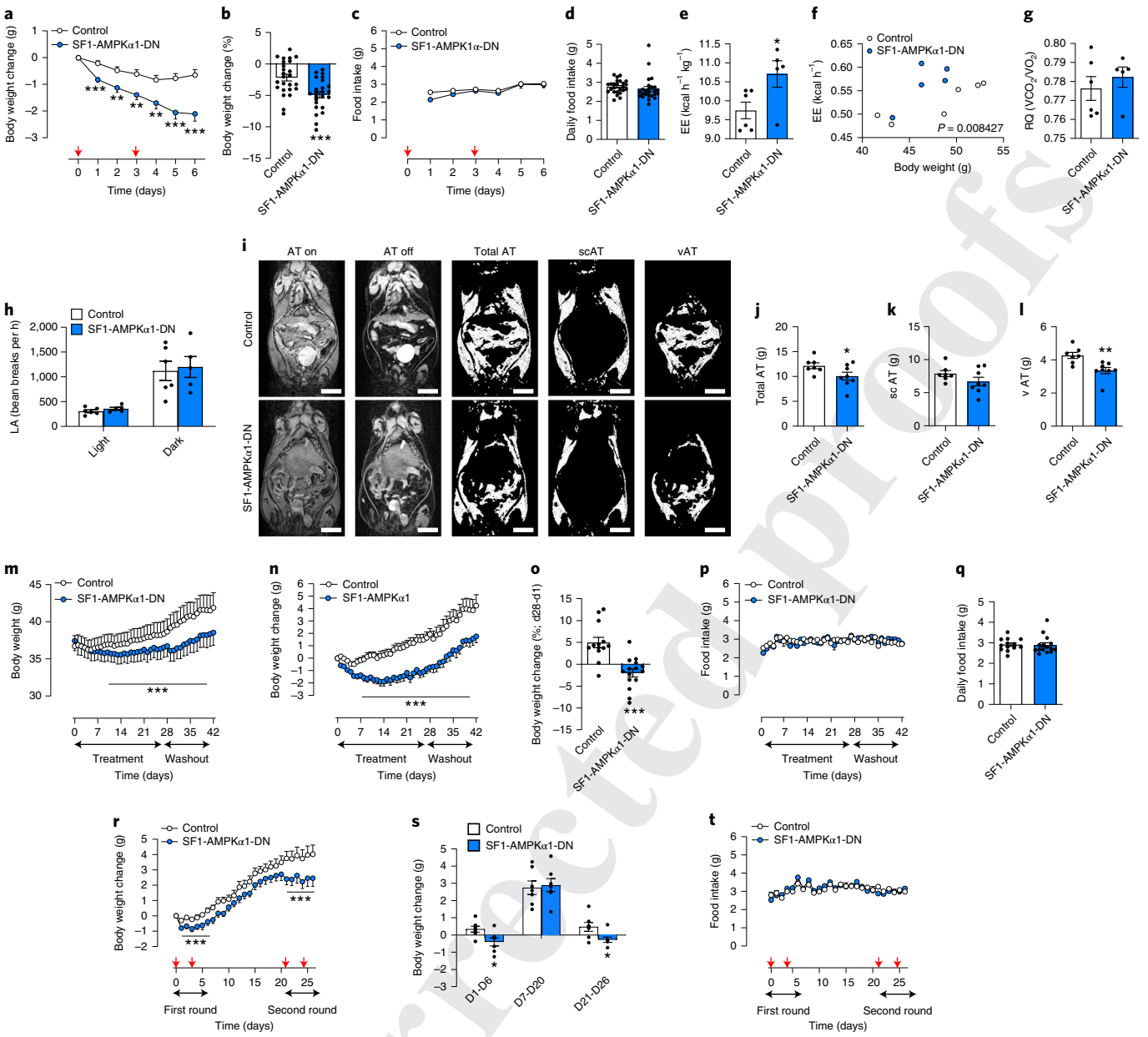

Fig. 4 | Effect of systemic treatment with SF1-AMPKα1-DN loaded sEVs on energy balance in DIO mice. a–**c**, Body weight change in grams (**a**, day 1, $P=0.00010$; day 2, $P=0.0037$; day 3, $P=0.0015$; day 4, $P=0.0018$; day 5, $P=8.84\times10^{-5}$; day 6, $P=8.92\times10^{-5}$), percentage (**b**, $P=0.00066$) and food intake (**c**) of mice after intravenous injection with control (non-loaded; $n=25$ mice) or SF1-AMPKα1-DN loaded ($n=24$ mice) sEVs. **d**, Daily food intake of mice after intravenous injection with control or SF1-AMPKα1-DN loaded sEVs every 3 d for 6 d ($n=25$ mice per group). **e**–**h**, Energy expenditure (EE, **e** $P=0.037$), ANCOVA (**f** $P=0.008427$) with body weight as covariate, respiratory quotient (RQ, **g**) and locomotor activity (LA, **h**) during light and dark phases of mice after intravenous VMH injection with control ($n=6$ mice) or SF1-AMPKα1-DN loaded sEVs ($n=5$ mice) every 3 d for 6 d. **i**–**l**, Representative NMR images (scale bars represent 2 cm) (**i**) and quantification (**j**) of adipose tissue (AT) on images with (AT on) and without fat (AT off), subcutaneous adipose tissue (scAT) and visceral AT (VAT) (**j**, total AT $P=0.028$; **l**, vAT $P=0.0045$) of mice after intravenous VMH injection with control ($n=7$ mice) or SF1-AMPKα1-DN loaded sEVs ($n=8$ mice) each 3 d for 6 d. **m**–**q**, Body weight (**m**, $P<0.001$) and body weight change in grams (**n**, $P<0.001$) and percentage (day 28 to day 1) (**o**, $P=7\times10^{-5}$), food intake (**p**) and daily food intake (**q**) of mice after intravenous injection with control or SF1-AMPKα1-DN loaded sEVs every 3 d for 28 d (control $n=13$ and SF1-AMPKα1-DN $n=15$ mice) and then 14 d of washout (control $n=6$ and SF1-AMPKα1-DN $n=8$ mice, as some animals were euthanized at day 28 for molecular analysis). **r**–**t**, Body weight changes during all treatment (**r**, days 1–6, $P<0.001$; days 21–26, $P<0.001$), during each period of treatment (**s**, days 1–6, $P=0.024$; days 21–26, $P=0.028$) and food intake (**t**) of mice after intravenous injection with control or SF1-AMPKα1-DN loaded sEVs ($n=7$ mice per group) every 3 d for 6 d, then 2 weeks of washout and again injections every 3 d for 6 d. In all panels, red arrows indicate injections. Data are expressed as mean ± s.e.m. $^*P<0.05$, $^{**}P<0.01$ and $^{***}P<0.001$ versus control. Statistical significance was assessed by a two-sided Student's *t*-test, except for total AT (**g**) where a one-sided Student's *t*-test was used.

(Extended Data Fig. 5h,i), therefore, excluding hepatic effects of sEVs. No changes were found either in key cardiovascular parameters, namely heart rate (Extended Data Fig. 5j) or arterial pressure (systolic, diastolic and mean; Extended Data Fig. 5k–m). If anything, blood pressure tended (although this was not significant) to be lower in the mice treated with SF1-AMPKα1-DN sEVs, which

was consistent with the weight loss evoked by this treatment. These data point to a lack of cardiovascular side effects of the AMPK-sEVs when given systemically.

Finally, to gain more insight into the time-dependent effect of SF1-AMPKα1-DN loaded sEV treatment, we performed a cross-over study. In this new experimental setting, animals were injected in the tail vein following a two-cycle protocol with an intercalated non-treatment period. Therefore, once the functional effect of the first injection was not observed anymore, new injections were performed to evaluate the potency of a new treatment. The data showed that both injection cycles induced the expected feeding-independent body weight loss (Fig. 4r–t).

Systemic SF1-AMPKα1-DN sEVs induce thermogenesis. Next, we examined whether the feeding-independent weight loss observed in DIO mice treated with SF1-AMPKα1-DN loaded sEVs might be linked to elevated BAT thermogenesis. This was justified by the fact that previous evidence has shown that genetic inhibition or ablation of AMPKα1 in those hypothalamic cells promoted brown fat activity[12–18,23] and by the data of our stereotaxic (Fig. 2e–h) and time-response experiments (Extended Data Fig. 4j). Mice treated with SF1-AMPKα1-DN loaded sEVs exhibited higher BAT temperature beginning at day 1 after injection that lasted for the entire treatment (Fig. 5a–c).

The presented evidence indicated that peripheral treatment with SF1-AMPKα1-DN loaded sEVs induced a BAT thermogenic-, but not feeding-, associated decrease in body weight. Therefore, before performing mechanistic experiments involving regulation of BAT function, we aimed to address the possible correlations between these variables. Our data revealed a highly significant negative correlation between body weight change and BAT temperature ($P<0.0001$): the mice that received the SF1-AMPKα1-DN loaded sEVs being the ones that lost most weight and had higher BAT temperature (Fig. 5d). Notably, food intake was similar in both groups and no association was found (Fig. 5e). Altogether, this evidence suggested that increased BAT function, leading to increased energy expenditure, accounted for the body weight-reducing effects of this sEV strategy. To gain further insight into the thermogenic effect of these sEVs targeting hypothalamic AMPK, we analysed BAT temperature in the crossover experiment (Fig. 4q–s). Notably, when the treatment was discontinued, the SF1-AMPKα1-DN loaded sEVs induced BAT temperature returned to control/basal values (Fig. 5f–h), indicating that the observed effect was time- and treatment-dependent. Further, we examined their impact on tail base temperature, a well-known thermoregulatory mechanism in rodents[39]. Loaded sEVs induced a slight, but not significant increase in the tail base temperature (Fig. 5i,j), indicating a tendency for heat dissipation by the tail.

Systemic SF1-AMPKα1-DN sEVs activate BAT. The BAT of SF1-AMPKα1-DN loaded sEV-treated DIO mice displayed increased protein levels of key thermogenic markers, such as UCP1, uncoupling protein 3 (UCP3) and peroxisome proliferator-activated receptor gamma coactivator 1 α and β (PGC1α and PGC1β) (Fig. 6a,b for 6 days treatment and Extended Data Fig. 6a for 28 days treatment). In keeping with this, injections of SF1-AMPKα1-DN loaded sEVs induced a higher BAT ^{18}F-FDG uptake when compared to liver (used as a control tissue) (Fig. 6c,d) indicating a higher BAT activation. The injection of SF1-AMPKα1-DN loaded sEVs was also associated with a non-significant trend to increase the browning of subcutaneous white adipose tissue (scWAT), as suggested by slightly increased UCP1 staining (Fig. 6e,f).

Overall, this evidence indicates that the systemic administration of SF1-AMPKα1-DN loaded sEVs targeting hypothalamic SF1 neurons induces changes in BAT activity. Notably, this action is probably not associated to an unspecific action of sEVs on brown adipocytes (where SF1 is not expressed) for two main reasons: (1) it has been recently reported that the inhibition of BAT AMPKα1 caused impairment rather than activation of this tissue[40] and (2) no changes in AMPK signalling were found in BAT after sEVs treatment either in vivo (Extended Data Fig. 4b) or when sEVs were given to primary BAT adipocytes in vitro (Extended Data Fig. 4c), excluding the existence of confounding unspecific actions. Moreover, no changes were found in the skeletal muscle thermogenic program (Extended Data Fig. 6b), indicating that the increase in energy expenditure observed on systemic administration of sEVs is driven by BAT and not muscular thermogenesis.

Systemic SF1-AMPKα1-DN sEVs activate SNS. BAT thermogenesis is mainly controlled by the SNS via β3 adrenoreceptors (β3-AR)[41–43]. Thus, we investigated whether the regulation of BAT following systemic injections of sEVs targeting AMPKα1 in VMH-SF1 neurons was mediated by the SNS. SF1-AMPKα1-DN loaded sEVs elevated total BAT sympathetic nerve traffic recorded directly by microneurography (Fig. 7a,b). Transection of the BAT nerve distal to the recording site allowed measurement of efferent sympathetic activity. Mice treated with SF1-AMPKα1-DN loaded sEVs displayed significantly elevated efferent BAT sympathetic nerve activity (SNA) relative to controls. However, the calculated afferent BAT nerve activity was not different between the two groups. These data demonstrate that SF1-AMPKα1-DN loaded sEVs stimulated efferent rather than afferent sympathetic outflow, which is consistent with a centrally mediated effect of the treatment. In keeping with SNA data, pharmacological inhibition of β3-AR by subcutaneous administrations of the specific β3-AR antagonist, SR5 9230A[12,13,15–18,44] prevented the decrease in body weight evoked by peripheral intravenous injection of SF1-AMPKα1-DN loaded sEVs

Fig. 5 | Effect of systemic treatment with SF1-AMPKα1-DN loaded sEVs on BAT thermogenesis in DIO mice. a–c, Representative BAT thermographic images, scale bars represent 1 cm (**a**), daily BAT temperature ($n=10$ mice per group; day 1, $P=0.030$; day 2 $P=0.0050$; day 3 $P=0.010$; day 4, $P=1.37\times10^{-5}$; day 5, $P=0.0023$; day 6, $P=9.88\times10^{-7}$) (**b**) and average BAT temperature quantification (control $n=69$ mice and SF1-AMPKα1-DN $n=68$ mice, $P=8.55\times10^{-12}$; box plot indicates median (middle line), 25th, 75th percentile (box) and 10th–90th percentiles (whiskers, minima and maxima, respectively)) (**c**) of mice injected in the tail vein with control (non-loaded) or SF1-AMPKα1-DN loaded sEVs every 3 d for 6 d. Red arrows indicate the injections. **d**,**e**, Correlation analyses between body weight changes in grams and BAT temperature (°C) (**d**) ($P<0.0001$) and food intake (**e**) ($n=60$ individual values per group) of mice injected in the tail vein with control (non-loaded) or SF1-AMPKα1-DN loaded sEVs each 3 d for 6 d. **f–h**, Representative BAT thermographic images at days 4, 14 and 23, scale bars represent 1 cm (**f**), daily BAT temperature time course (**g**) (day 1, $P=0.0027$; day 2, $P=0.040$; day 3, $P=0.00035$; day 4, $P=0.0024$; day 22, $P=0.0033$; day 23, $P=0.038$; day 24, $P=0.00089$) and daily BAT temperature histograms (**h**, days 1–6, $P=0.00013$; days 22–25, $P=0.0041$) of mice after intravenous injection with control (non-loaded) or SF1-AMPKα1-DN loaded sEVs ($n=8$ mice per group) every 3 d for 6 d, then 2 weeks of washout and again injections every 3 d for 6 d. BAT temperatures were not monitored at days 21 and 26 to avoid any kind of stress. **i**,**j**, Representative tail base thermographic images, scale bars represent 1 cm (**i**) and average tail base temperature quantification (**j**) of mice after intravenous injection with control (non-loaded) or SF1-AMPKα1-DN loaded sEVs ($n=8$ mice per group) every 3 d for 6 d, then 2 weeks of washout and again injections every 3 d for 6 d. Data are expressed as mean ± s.e.m. $^{*}P<0.05$, $^{**}P\leq0.01$ and $^{***}P<0.001$ versus control. Statistical significance was assessed by a two-sided Student's *t*-test; except for BAT Temp at days 2 and 23 in the crossover experiment (**g**) where a one-sided Student's *t*-test was used.

without interfering with feeding (Fig. 7c-d). Consistent with the increased weight gain after the β3-AR blockade, the treatment with SR59230A abrogated the increase in BAT temperature (Fig. 7e,f) and UCP1 protein levels (Fig. 7g,h). Of note, when given alone, SR59230A did not promote any changes in any of the analysed parameters (control + vehicle versus control + SR59230A: (1) body

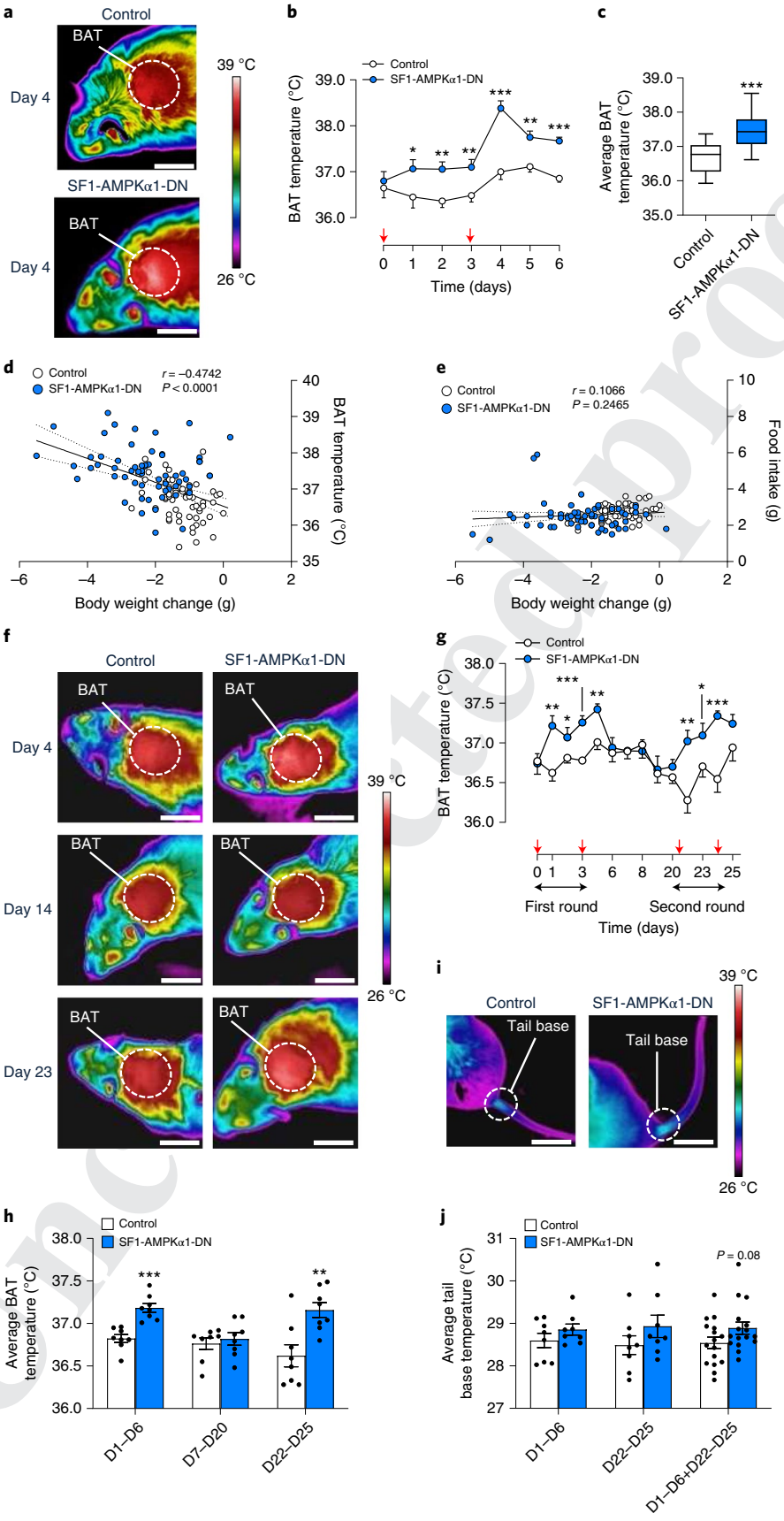

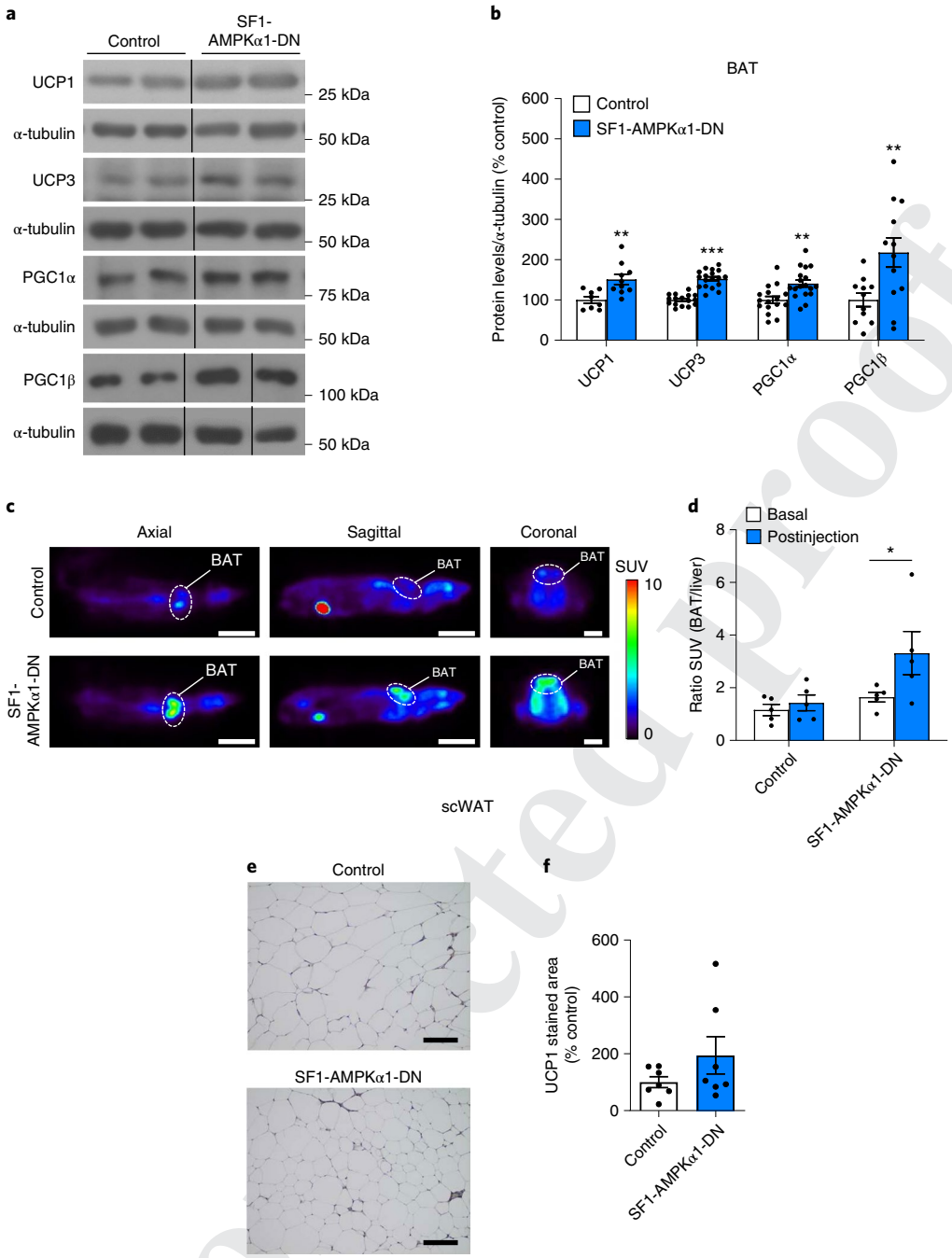

Fig. 6 | Effect of systemic treatment with SF1-AMPKα1-DN loaded sEVs on thermogenic pathways in DIO mice. a,**b**, Representative UCP1, UCP3, PGC1α and PGC1ß western blot images (**a**) and quantification of their expression (**b**) in BAT of mice after intravenous injection with control (non-loaded; UCP1 $n=8$ mice; UCP3 $n=16$ mice; PGC1α $n=16$ mice; PGC1β $n=11$ mice) or SF1-AMPKα1-DN loaded sEVs (UCP1 $n=10$ mice; UCP3 $n=18$ mice; PGC1α $n=18$ mice; PGC1β $n=12$ mice) every 3 d for 6 d. α-tubulin was used as control of protein loading. UCP1 $P=0.0051$; UCP3 $P=1.41\times10^{-9}$; PGC1α $P=0.0023$; PGC1β $P=0.001$. A black line was inserted on the immunoblots when samples were loaded on the same gel, but not side by side. **c**,**d**, Representative axial (scale bars represent 2 cm), sagittal (scale bars represent 2 cm) and coronal (scale bars represent 1 cm), PET–CT scan images showing BAT (**c**) and the ratio of the SUV BAT/liver (**d**) at the basal level and after injection with control (non-loaded) or SF1-AMPKα1-DN loaded sEVs ($n=5$ mice per group); Postinjection $P=0.031$. **e**,**f**, Representative scWAT immunohistochemistry with anti-UCP1 antibody showing UCP1 staining (**e**) and quantification (**f**) of UCP1 stained area in scWAT from mice after injection with control (non-loaded) or SF1-AMPKα1-DN loaded sEVs ($n=7$ mice per group); scale bars represent 100 µm. Data are expressed as mean ± s.e.m. $^{*}P<0.05$, $^{**}P<0.01$ and $^{***}P<0.001$ versus control. Statistical significance was assessed by a two-sided Student's *t*-test; except for SUV at postinjection (**d**) where a one-sided Student's *t*-test was used.

weight: −1.27 ± 0.09 versus −1.30 ± 0.42, non-significant; (2) food intake: 2.49 ± 0.07 versus 2.58 ± 0.17, non-significant; (3) BAT temperature: 36.8 ± 0.18 versus 36.7 ± 0.07, non-significant; (4) UCP1 BAT: 100 ± 8.2 versus 84.1 ± 8.3, non-significant). Overall, this evidence indicates that the systemic injection of SF1-AMPKα1-DN loaded sEVs promotes weight loss, independently of feeding, acting on SF1 neurons of the VMH, leading to increased BAT thermogenesis through the SNS via β3-AR activation. Notably, the fact that,

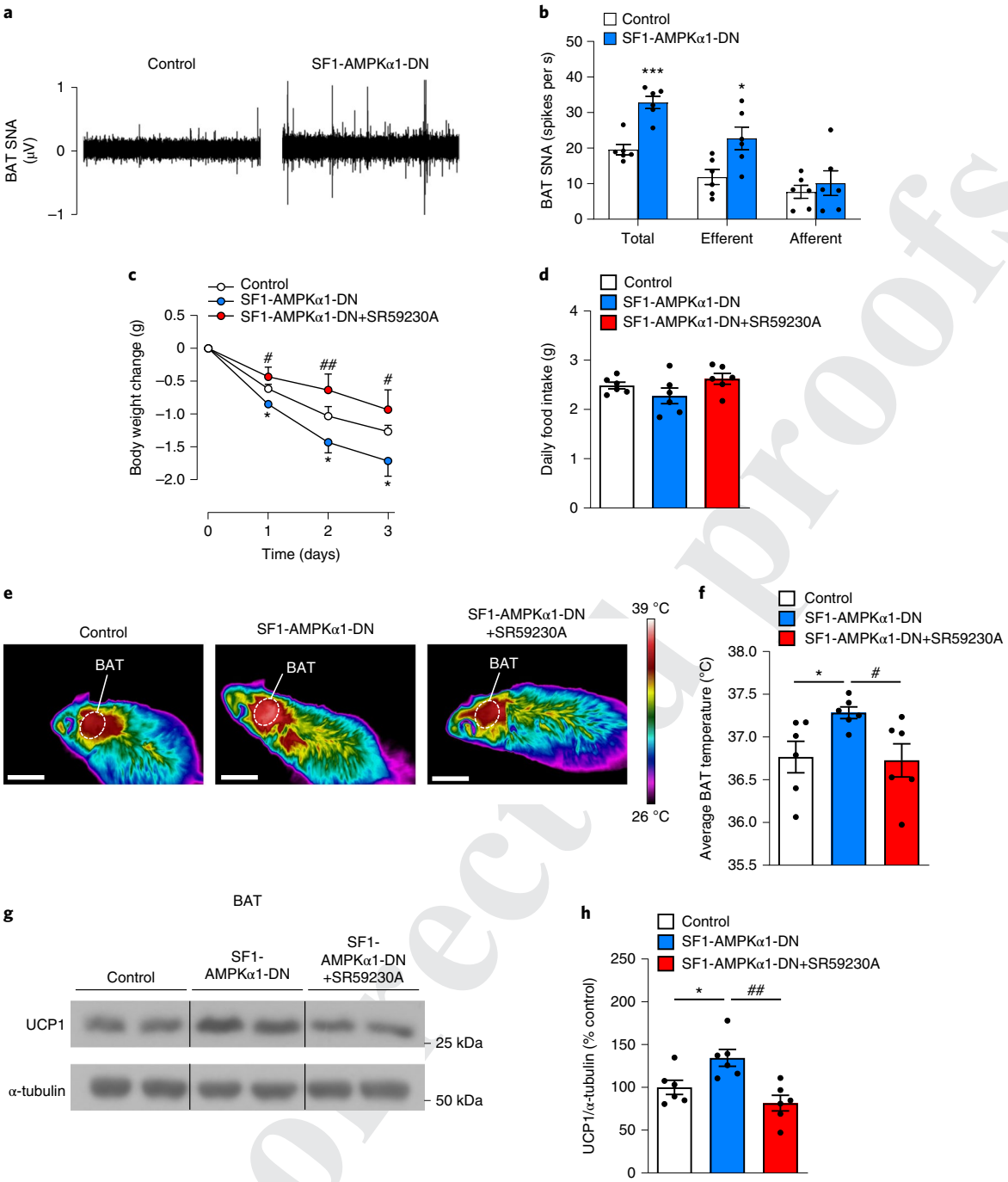

Fig. 7 | Effect of adrenergic blockade on the systemic treatment with SF1-AMPKα1-DN loaded sEVs in DIO mice. a,**b**, Representative BAT SNA tracings (**a**) and its quantification (**b**) (total, efferent and afferent signals) in spikes per s of DIO mice injected in the tail vein with control (non-loaded) or SF1-AMPKα1-DN ($n = 6$ mice per group) sEVs for 24 h; total $P = 0.00016$; efferent $P = 0.017$. **c**–**f**, Body weight changes (**c**, day 1 control versus SF1-AMPKα1-DN $P < 0.05$, SF1-AMPKα1-DN versus SF1-AMPKα1-DN + SR59230A $P < 0.05$; day 2 control versus SF1-AMPKα1-DN $P < 0.05$, SF1-AMPKα1-DN versus SF1-AMPKα1-DN+SR59230A $P < 0.01$; day 3 control versus SF1-AMPKα1-DN $P < 0.05$, SF1-AMPKα1-DN versus SF1-AMPKα1-DN+SR59230A $P < 0.05$) daily food intake (**d**), representative BAT thermographic images, scale bars represent 2 cm (**e**) and average BAT temperature quantification (**f**, control versus SF1-AMPKα1-DN $P < 0.05$, SF1-AMPKα1-DN versus SF1-AMPKα1-DN+SR59230A $P < 0.05$) of mice injected with control (non-loaded), SF1-AMPKα1-DN loaded sEVs alone or in the presence of the specific β3-AR antagonist, SR59230A ($n = 6$ mice for each treatment). **g**,**h**, Representative UCP1 western blot images (**g**) and quantification of its expression (**h**, control versus SF1-AMPKα1-DN $P < 0.05$, SF1-AMPKα1-DN versus SF1-AMPKα1-DN+SR59230A $P < 0.01$) in BAT of mice after intravenous injection with control (non-loaded), SF1-AMPKα1-DN loaded sEVs alone or in the presence of the specific β3-AR antagonist, SR59230A ($n = 6$ mice for each treatment). α-tubulin was used as control of protein loading. A black line was inserted on the immunoblots when samples were loaded on the same gel, but not side by side. Data are expressed as a mean ± s.e.m. $^{*}P < 0.05$, $^{**}P < 0.01$ and $^{***}P < 0.001$ versus control; $^{\#}P < 0.05$ and $^{\#\#}P < 0.01$ SF1-AMPKα1-DN versus SF1-AMPKα1-DN+SR59230A. Statistical significance was assessed by two-sided ANOVA.

as shown, no changes were found in key cardiovascular parameters (Extended Data Fig. 5j–m) suggested that the sympathetic stimulation exerted by the sEVs was specific for BAT.

Systemic SF1-AMPKα1-DN sEVs activate BAT on thermoneutrality. We aimed to investigate whether the effect of SF1-AMPKα1-DN loaded sEVs was dependent on the ambient temperature since in a non-thermoneutral environment (22–23 °C as mice are housed) the basal activation of BAT[41,45] could mask the effects of sEVs. However, the data showed that treatment with SF1-AMPKα1-DN loaded sEVs in DIO mice housed in thermoneutral conditions (30 °C) elicited a marked body weight reduction (Fig. 8a,b), independently of feeding (Fig. 8c-d), and associated with increased BAT thermogenesis (Fig. 8e,f) and BAT UCP1 protein content (Fig. 8g,h). Overall, this evidence demonstrates that SF1-AMPKα1-DN loaded sEVs modulate energy balance and body weight by targeting BAT thermogenesis.

UCP1 is essential for systemic SF1-AMPKα1-DN sEVs. Finally, we investigated whether the effect of SF1-AMPKα1-DN sEVs on BAT thermogenesis and body weight was dependent on UCP1 expression. While SF1-AMPKα1-DN sEVs induced a feeding-independent but thermogenesis-dependent body weight decrease in wild-type mice (Figs. 8i,k,m,n), this effect was totally absent in *ucp1* null mice (Figs. 8j,l,o,p). These data demonstrate that UCP1 plays an essential role in mediating the central effects of SF1-AMPKα1-DN sEVs on thermogenesis and energy balance, and simultaneously confirm that the contributions from other peripheral tissues such as muscle are negligible.

Discussion

The development of strategies to hinder the current obesity pandemic has been hampered mainly due to: (1) the intrinsic redundancy of the homeostatic mechanisms modulating body weight, (2) the resilience to homeostatic perturbations, as a result of counter-regulatory responses (that is, decreased feeding leads to reduced energy expenditure), (3) the limited specificity of most drugs so far available and (4) adverse side effects[1–5]. Thus, it would be interesting to generate new genetic strategies/resources that would permit a more precise targeting, and therefore higher specificity.

Owing to their composition, sEVs can be used as shuttles of drugs and, thus, to carry molecules towards specific cells[19–22], therefore being exploited for prognosis, biomarkers and innovative therapies[19–22,24–26]. In fact, their properties, such as biocompatibility and low immunogenicity, make them ideal for reaching the CNS[27,28]. To target the central mechanism modulating energy balance, the crossing of the BBB is a major challenge in delivering agents of interest. To circumvent this limitation, engineered sEVs expressing the RVG peptide fused to Lamp2b at their surface have been developed, allowing specific neuronal targeting[28], however, without being specific to one neuronal population of any given brain region. We took advantage of this approach using sEVs as cargos of a DNA plasmid of interest in an obesity-driven context. Therefore, in this study, we developed sEVs as delivery tools for targeting a central and canonical pathway modulating energy balance, namely hypothalamic AMPK[3,8,11], specifically in SF1 neurons of the VMH.

Notably, AMPK actions exhibit a high anatomic and isoform-dependent specificity; while anorexia is elicited by the selective ablation of the AMPKα2 isoform in agouti-related protein neurons of the hypothalamic arcuate nucleus (ARC)[46], the inhibition of AMPKα1 activity in SF1 neurons of the VMH increases energy expenditure by stimulating SNS-driven BAT thermogenesis[17,18]. Of note, mice with selective ablation of AMPKα1 in SF1 neurons are resistant to DIO[18], which suggests that targeting this isoform in that hypothalamic population might be an interesting target against obesity. However, the implementation of this strategy required a high level of hypothalamic specificity as any side effect related to peripheral inhibition of AMPK would have the opposite effect, worsening insulin resistance and diabetes[3,47,48], thus raising the importance of the specificity of the treatment. Therefore, we developed sEVs exogenously loaded with a plasmid encoding for an AMPKα1-DN mutant under the control of SF1 promoter. Notably, to circumvent any central/brain manipulation, and to be in a condition that would be acceptable for a potential therapeutically use, these sEVs were peripherally administered in the tail vein. The data showed that SF1-AMPKα1-DN loaded sEVs promoted a marked feeding-independent weight-reducing effect due to increased SNS-mediated UCP1-dependent BAT thermogenesis (as demonstrated by the lack of effect in *ucp1* null mice) and increased energy expenditure, and not associated with either systemic inflammatory responses or hepatic and cardiovascular side effects. A possible limitation of our study is that we have analysed the energy expenditure in the 6-day treatment setting, but not in other settings, such as the long-term and thermoneutrality studies. In this regard, the fact that the action occurs in the absence of appetite compensatory changes in the SF1-AMPKα1-DN loaded sEVs injected mice has translational relevance because it excludes undesired rebound effects, which typically characterize dietary interventions[5], as demonstrated also by our long-term and crossover treatments.

Despite reaching peripheral tissues, SF1-AMPKα1-DN loaded sEVs only modulated AMPK signalling in the VMH, and specifically in SF1 neurons, as demonstrated by our colocalization analyses. This is due to (1) the RVG-mediated tropism for neurons[28] and (2) the SF1-driven expression of the AMPKα1-DN transgene. Of note, no detectable changes in AMPK activity were found in (1) other hypothalamic neighbouring nuclei, (2) peripheral SF1-expressing

Fig. 8 | Effect of systemic treatment with SF1-AMPKα1-DN loaded sEVs on energy balance in thermoneutral conditions and UCP1 knockout mice under HFD. a,**b**, Body weight change in grams (**a**; day 1, $P=0.023$; day 2, $P=0.034$; day 3, $P=0.045$; day 4, $P=0.009$; day 5, $P=0.03$; day 6, $P=0.002$) and in percentage at day 6 (**b**, $P=0.0015$) of mice after intravenous injection with control (non-loaded) or SF1-AMPKα1-DN loaded sEVs ($n=9$ mice per group) every 3 d for 6 d placed under thermoneutrality (30 °C). **c**,**d**, Food intake (**c**) and daily food intake (**d**) of mice after intravenous injection with control (non-loaded) or SF1-AMPKα1-DN loaded sEVs ($n=9$ mice per group) every 3 d for 6 d placed at 30 °C. **e**,**f**, Representative BAT thermographic images, scale bars represent 2 cm (**e**) and BAT temperature quantification (**f**) of mice after intravenous injection with control (non-loaded) or SF1-AMPKα1-DN loaded sEVs ($n=9$ mice per group) every 3 d for 6 d, placed under thermoneutral conditions; $P=0.012$. **g**,**h**, Representative UCP1 western blot images (**g**) and quantification of UCP1 expression (**h**) in BAT of mice after intravenous injection with control (non-loaded, $n=5$ mice) or SF1-AMPKα1-DN loaded sEVs ($n=7$ mice) every 3 d for 6 d. $P=0.0061$. α-tubulin was used as control of protein loading. A black line was inserted on the immunoblots when samples were loaded on the same gel, but not side by side. **i**,**j**, Body weight change of wild-type (*ucp1*$^{+/+}$, **i**, $n=6$ mice; day 1 $P=0.035$; day 2 $P=0.028$) and *ucp1* null mice (*ucp1*$^{-/-}$, **j**, $n=10$ mice) after a single intravenous injection with control (non-loaded) or SF1-AMPKα1-DN loaded sEVs. Red arrows indicate the injections. **k**,**l**, Daily food intake of wild-type (**k**, control $n=6$ mice and SF1-AMPKα1-DN $n=7$ mice) and *ucp1* null mice (**l**, $n=10$ mice) after a single intravenous injection with control (non-loaded) or SF1-AMPKα1-DN loaded sEVs. **m**–**p**, Representative BAT thermographic images, scale bars represent 1 cm (**m**,**o**) and BAT temperature interscapular temperature quantification (**n**,**p**) of wild-type (**m**,**n**, $n=7$ mice per group, $P=0.019$) and *ucp1* null mice (**o**,**p**, $n=10$ mice per group) after a single intravenous injection with control (non-loaded) or SF1-AMPKα1-DN loaded sEVs. Data are expressed as mean ± s.e.m. $^{*}P<0.05$, $^{**}P<0.01$ and $^{***}P<0.001$ versus control. Statistical significance was assessed by a two-sided Student's *t*-test.

tissues, such as the testis, the adrenal gland and the pituitary, and (3) peripheral non-expressing SF1 tissues, such as the liver, BAT, heart and skeletal muscle. Overall, these data indicate that the systemic treatment with SF1-AMPKα1-DN loaded sEVs that we have developed was able to induce weight loss by specifically inhibiting AMPKα1 function in SF1 neurons of the VMH. This demonstrates

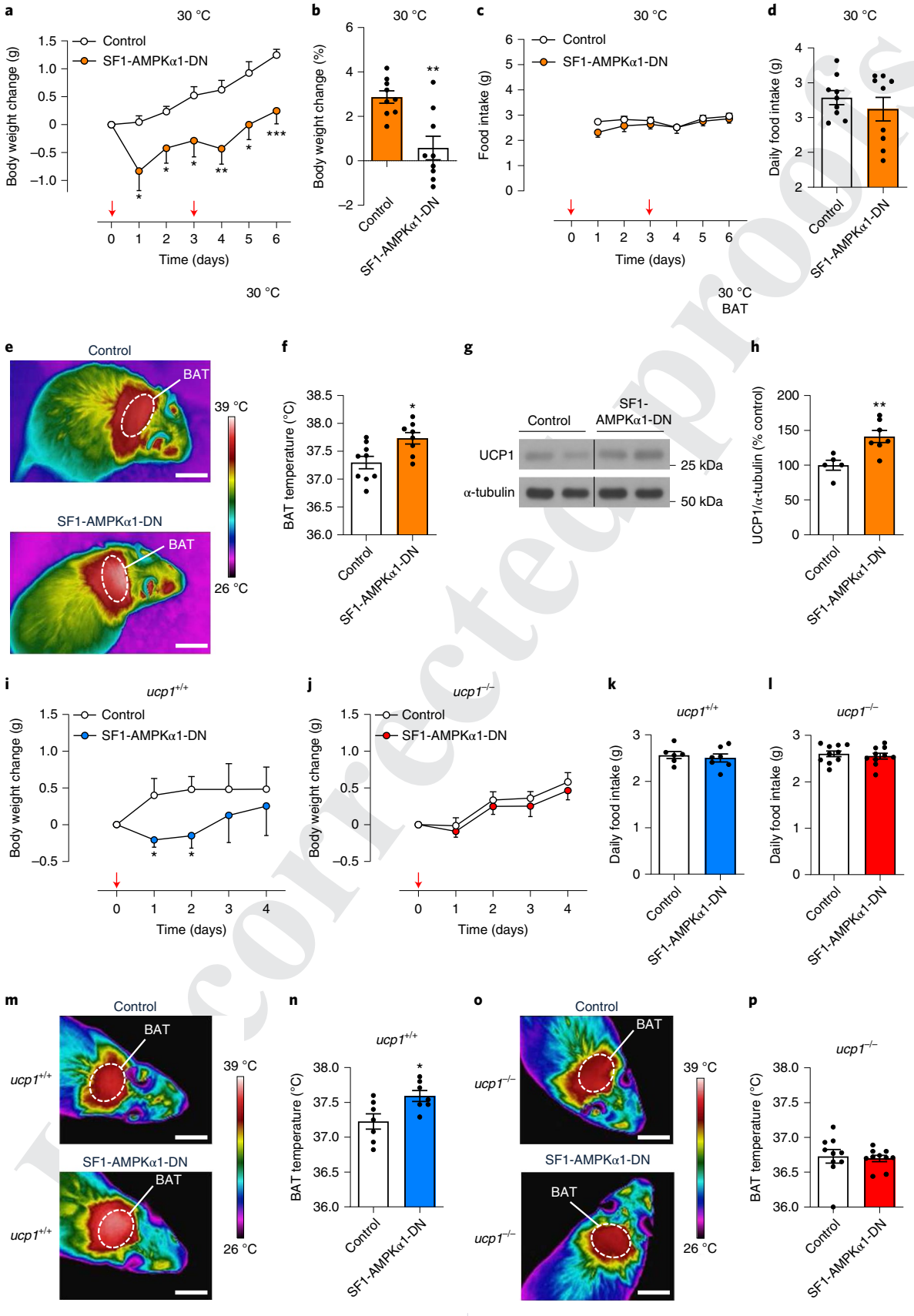

that hypothalamic networks can be selectively targeted by peripherally conveyed agents, which opens a new therapeutic possibility for obesity and other neurological disorders. To reinforce this idea, our data also showed lack of hepatic and cardiovascular side effects of the AMPK-sEVs when given systemically. This indicates that targeting of hypothalamic AMPK could bypass some of the secondary effects associated to treatments acting peripheral mechanism regulating energy balance and metabolism[5].

Strategies for the development of successful treatments against obesity have been mainly focused on peripheral approaches, given the intrinsic complexity of targeting the brain. However, the growing knowledge on the hypothalamic mechanisms controlling energy homeostasis has made evident that the specific modulation of neural circuits in discrete areas may offer new and more effective targets for drug development. Many of the key players in energy balance that were the basis for the development of new treatments of obesity (leptin, ghrelin, glucagon-like peptide-1 agonists, glucagon and so on)[1–6] are likely to act through hypothalamic AMPK[3]. However, targeting specific neurons in the CNS was considered a daunting task. Here, we provide evidence about the capacity of sEVs to be used as natural bio-carriers as an alternative to more traditional delivery systems in the treatment of obesity, limiting inflammatory responses and enhancing a highly selective cellular action, namely AMPKα1 in SF1 neurons in the VMH. Thus, sEVs harbouring genetic tools open a new way in the rational design of new strategies for the treatment of obesity and associated comorbidities and perhaps other neurological diseases.

Methods

Cell culture. The JAWS II dendritic cell line was purchased from the American Type Culture Collection (CRL-1194, ATCC). The GT1-7 and the Neuro2A cell lines were provided by E. Domínguez (University of Santiago de Compostela (USC), Spain) and by INSERMU1066 (University of Angers, France), respectively. Immortalized brown adipocytes were obtained from C57BL/6J mice as reported[49]. Primary cortical astrocytes were obtained from cerebral cortices of 3-d-old C57BL/6J mice and maintained in culture for 4–6 d.

Animals. Adult (8–12 weeks) male C57BL/6J mice (25 g; Centro de Biomedicina Experimental; Santiago de Compostela, Spain or Jackson Laboratory, USA), nude mice (NRj:NMRI-Foxn1nu/Foxn1nu; Janvier Laboratories) and C57BL/6J and C57BL/6N homozygous UCP1 knockout (UCP1-KO, *ucp1*$^{-/-}$) males and their corresponding wild-type littermates[50] (University of Lübeck, Germany) were used; with no differences in the recorded parameters between the substrains. Animals were housed with an artificial 12-h light (8:00 to 20:00)/12-h dark cycle, under controlled temperature and humidity conditions and allowed to free access to a regular chow diet or 60% HFD (D12492; Research Diets, Inc.) and filtered tap water for 10 weeks. The experiments were performed in agreement with the International Law on Animal Experimentation and were approved by the USC Ethical Committee (Project ID 15010/14/006 and 15012/2020/010), the University of Iowa Animal Research Committee (Protocol 8101549) and MELUR Schleswig Holstein (77/7-19).

Plasmids. The plasmid encoding for Lamp2b[28] sequence (provided by S. Yiqi, University of Oxford, UK) containing NheI and BamHI restriction sites was cloned into a pEGFP-C1 backbone, taking care to remove eGFP encoding sequence. RVG primers (forward 5′-TCGATACACCATTTGGATGCCCGAGAATCCGA GACCAGGGACACCTTGTGACATTTTTACCAATAGCAGAGGGAAGAGAG CATCCAACGGGT-3′; reverse 5′-CCGGACCCGTTGGATGCTCTCTTCCCTC TGCTATTGGTAAAAATGTCACAAGGTGTCCCTGGTCTCGGATTCTCGGG CATCCAAATGGTGTA-3′) were inserted between XhoI and BspEI at the N terminus of Lamp2b. The SF1-AMPKα1-DN plasmids were purchased from Viraquest.

sEV generation and isolation. JAWS II cells were seeded at 5×10^6 cells in T75 flasks the day before the transfection. On the transfection day, JAWS II cells were transiently transfected with Lamp2b-RVG plasmids using MacsFectin (Miltenyi Biotec). Then 20 µg of Lamp2b-RVG plasmid/350 µl of serum-free medium were added to 40 µl of MacsFectin/350 µl of serum-free medium. The mixtures were incubated for 20 min at room temperature to allow the formation of transfection complexes before being added to the cells. After 24 h, the cell medium was replaced by FBS-sEV-free medium. After 48 h, the supernatant was collected, centrifuged at 300*g* and 2,000*g* for 10 min. The resultant supernatant was centrifuged at 20,000*g* for 30 min to exclude large EVs. sEV pellets were further isolated by a 200,000*g* centrifugation step for 2 h at 4 °C using a MLA-50 rotor (Optima Max-XP ultracentrifuge; Beckman Coulter). sEV pellet was washed with PBS using the same ultracentrifuge process before being resuspended in PBS and kept at −80 °C.

Electron microscopy. sEVs were fixed overnight in 2.5% paraformaldehyde (PFA) in 0.1 M sodium cacodylate buffer (pH 7.4). sEVs were pelleted using above-described ultracentrifugation process and resuspended in 2.5% glutaraldehyde solution. sEVs were deposited on copper grids and negatively stained with phosphotungstic acid and observed with a JEM1400 Transmission Electron Microscope (JEOL) at 200 kV.

NTA. Here, 50 µg of purified (1) native non-modified, (2) Lamp2b-RVG neuronal-targeted or (3) Lamp2b-RVG SF1-AMPKα1-DN loaded sEVs were diluted in PBS, and size distribution was analysed at 37 °C using the NanoSight NS 300 (Malvern Instruments). Briefly, 60-s videos were recorded and analysed by the NTA software.

sEVs loading and evaluation of nucleic content. sEVs (50–300 µg) were incubated with 10 µl of Exo-Fect solution (System Biosciences), 20 pmol siRNA-Texas Red (System Biosciences) or 5 µg of plasmid (GFP or SF1-AMPKα1-DN) and 70 µl of PBS for 10 min at 37 °C. Then, after adding 30 µl of Exo-Quick solution (System Biosciences), the mixture was placed at 4 °C for 30 min. The samples were then centrifugated for 3 min at 14,000*g* to pellet the sEVs before being resuspended in PBS. sEVs were either used directly or stored at −80 °C.

To evaluate the loading with the SF1-AMPKα1-DN plasmid, purified SF1-AMPKα1-DN loaded sEVs were treated or not with DNase I (RNase free, Qiagen) diluted in RDD buffer in absence or presence of 0.2% Triton X-100 (ThermoFisher Scientific, Inc.) at 37 °C for 10 min. To inactivate DNase activity, the samples were heated at 75 °C for 10 min. Both non- and DNA-digested sEVs were then subjected to end-point PCR in the presence of AMPK or glyceraldehyde 3-phosphate dehydrogenase (GAPDH) (as control) primers. The PCR reaction products were then run on a 2% agarose gel (Sigma-Aldrich) containing 0.001% ethidium bromide. The gels were visualized in the ultraviolet light in an INFINITY VX2 1120 M Gel Documentation System (Vilber Lourmat). AMPK, forward 5′-ACGGCCGAGAAGCAGAAGCAC-3′; reverse 5′-TCGTGCTTGCCCACCTTCAC-3′ and GAPDH: forward 5′-AGTATGTCGTGGAGTCTAC-3′; reverse 5′-CATACTTGGCAGGTT TCTC-3′.

sEVs labelling and bio-distribution analysis. sEVs were incubated with 5 µg ml^{-1} of Vybrant DiD Cell (excitation maximum 644 nm, emission maximum 665 nm) (Molecular Probes) in PBS for 10 min at room temperature, washed twice in PBS with a 200,000*g* ultracentrifuge step for 2 h. The resultant DID-labelled sEVs were recovered in PBS. Then 100 µg of DID-labelled native or Lamp2b-RVG sEVs were injected intravenously in nude mice. For the analysis of DID-labelled sEVs bio-distribution, the multispectral imaging system MAESTRO In Vivo Fluorescence Imaging System (Cambridge Research and Instrumentation) was used. DID-labelled sEV bio-distribution was analysed at different times (30 min, 2, 4 and 6 h) on isoflurane-sedated mice. The respective fluorescence of isolated organs (liver, spleen, lungs, heart, brain and skeletal muscle) was also analysed following the euthanasia of the animal.

In vitro treatment with sEVs. Twenty-four hours before treatments with sEVs, (1) JAWS II cells were plated at 2×10^4 cells in µ-Slide 8 Well (Ibidi), (2) GT1-7 and (3) Neuro2A cells were seeded in six-well plates at 2×10^5 cells and (4) primary cortical astrocytes were plated at 5×10^5 cells. Then, JAWS II cells were incubated with either non-loaded sEVs, siRNA-Texas Red- or GFP-loaded sEVs (1 µg ml^{-1} for all conditions) before being fixed and the respective fluorescence was evaluated at different times (2, 6 and 24 h) by confocal microscopy (CLMS 700, Zeiss, ZEN fluorescence). On the other side, GT1-7, Neuro2A cells, brown adipocytes and primary cortical astrocytes cells were treated with 10 µg ml^{-1} of SF1-AMPKα1-DN loaded sEVs for 24 h before being collected and protein extracted for later analysis.

Stereotaxic treatment with sEVs. DIO mice were placed in a stereotaxic frame (David Kopf Instruments) under ketamine-xylazine anaesthesia (50 mg kg^{-1}, intraperitoneal). The VMH was targeted bilaterally using a 32-gauge needle (Hamilton)[17,18]. Then 2 µg of control- or SF1-AMPKα1-DN loaded sEVs were delivered at a rate of 100 nl min^{-1} for 10 min (0.5 µl at each injection site).

Systemic treatment with sEVs. Here, 100 µg of non- or SF1-AMPKα1-DN loaded sEVs were injected in the tail vein of the mice each 3 d for corresponding times depending on the experiments. For the time course experiments (both SF1-AMPKα1-DN plasmid in vivo expression and UCP1 BAT expression time courses), the mice were injected once and euthanized at corresponding time points (24 h, 48 h, 72 h and 1 week). The β3-AR specific antagonist SR59230A ((3-(2-ethylphenoxy)-1-((1,*S*)-1,2,3,4-tetrahydronapth-1-ylamino]-2*S*-2-propanol-oxalate) (3 mg kg^{-1} d^{-1} in dimethylsulfoxide, Tocris Bioscience)[12,13,15–18,44] was administrated subcutaneously twice a day, starting 3 d before the first

intravenous injection. For the thermoneutrality experiments, the mice were housed at thermoneutral conditions (30 °C) and allowed to adapt to the temperature fluctuations (2 °C increase every day for 4 d).

Temperature measurements. Skin temperature surrounding BAT and temperatures of tail base were recorded with an infrared camera (B335: compact infrared thermal-imaging camera, FLIR) and analysed with a specific software package (FLIR-Tools-Software, FLIR). In all cases, the average temperature of the selected area was chosen[13,15–18,44].

Indirect calorimetry. Animals were analysed for energy expenditure, oxygen consumption (VO_2), respiratory quotient and locomotor activity using a calorimetric system (LabMaster, TSE Systems)[13,15–18,44,51].

NMR. All studies were conducted on a 9.4 T horizontal bore magnet (Bruker BioSpin;) with 440 mT m^{-1} gradients. A quadrature volume coil (7 cm in diameter) was used for body composition. NMR procedures were carried out under sevoflurane anaesthesia (6% induction and 3.5% maintenance in a gas mixture of 70% NO_2/30% O_2). For body composition studies, fast low angle shot sequences with repetition time/echo time of 1,300 per 3.5 ms, number of averages was two, 30 coronal slices of 1 mm, field of view was 60 × 80 mm and matrix size of 256 × 350 (in plane resolution of 0.234 × 0.229 mm $pixel^{-1}$) were acquired with and without fat suppression option to generate both 'fat suppression' and 'fat' image sets. Total acquisition time was 31 min. The magnetic resonance postprocessing was performed using ImageJ software (W. Rasband). Semiautomatic image processing was used to create fat masks (volumes of total (total AT), subcutaneous adipose tissue (scAT) and visceral adipose tissue (vAT)) comparing coregistered image sets with and without fat suppression option. Using a standard density for adipose tissue (0.9 g ml^{-1}) and other tissues (1.04 g ml^{-1}), we converted the magnetic resonance imaging volumes to weights[52–54].

Positron emission tomography–computed tomography (PET–CT). Whole-body microPET–CT images were acquired with the Albira PET/CT Preclinical Imaging System (Bruker Biospin). Mice received an injection of (7.4 ± 1.85) MBq of 2-^{18}F-fluoro-2-deoxy-2-glucose (^{18}F-FDG) in the tail vein. The acquisition was performed 45 ± 10 min after the ^{18}F-FDG injections. Images were generated by using the Bruker Albira Suite Software. The brown fat and liver areas were delineated by using image tools implemented the AMIDE Software (http://amide.sourceforge.net/) to generate a three-dimensional spherical volume of interest with radius of 6 mm. Thus, mean standardized uptake values (SUV) were calculated[17,18].

SNA recording. Multi-fibre recording of SNA was obtained from the nerve subserving BAT[12,15,17,18,55]. Each mouse was anaesthetized and then equipped for direct multi-fibre SNA from the nerves serving the subscapular BAT. A bipolar platinum-iridium electrode (36-gauge, A-M Systems) was suspended under the nerve and secured with silicone gel (Kwik-Sil, WPI). The electrode was attached to a high-impedance probe (HIP-511, Grass Instruments) and the nerve signal was amplified at 10^5 times and filtered at 100 and 1,000 Hz cutoffs with a Grass P5 AC preamplifier. The amplified and filtered nerve signal was routed to a speaker system and to an oscilloscope (model 54501A, Hewlett-Packard) to monitor the audio and visual quality of the BAT sympathetic nerve recordings for quantification purposes. The amplified, filtered nerve signal was also directed to a MacLab analogue–digital converter (Model 8S, ADInstruments) containing the software (MacLab Chart Pro, v.7.0). Under a stable isothermal (37.5 °C) condition and anaesthesia, baseline BAT SNA was recorded over a 30-min period. The nerve was then cut distally to record the efferent SNA during another 15 min. Next, the background noise was subtracted to measure real SNA, by recording the activity remaining after cutting the nerve proximal to the recording site. Afferent nerve activity was determined by subtracting the efferent from total nerve activity. During nerve recording, systolic, diastolic and mean arterial pressure along with heart rate were measured.

Sample processing. Mice were killed by cervical dislocation and decapitation, and tissues were immediately homogenized on ice. Samples and serum were stored at −80 °C. We conducted dissection of the VMH using a micro-punch procedure under the microscope[12,13,15–18,44].

Blood biochemistry. LH serum levels were measured in duplicate using a double-antibody method and radioimmunoassay kits, supplied by A.F. Parlow (National Institute of Diabetes and Digestive and Kidney Diseases National Hormone and Peptide Program)[15,56]. Serum testosterone and CORT levels were measured using RIA kits (MPBiomedicals, LLC). Leptin circulating levels were measured using a mouse enzyme-linked immunosorbent assay kit (no. EZML-82K, Millipore). Cholesterol (no. 1001093, Spinreact), triglycerides (no. 1001314, Spinreact), free fatty acids (NEFA Standard 270-77000 and NEFA-HR R2 set 436-91995 WAKO) circulating levels and AST (no. 41272, AST) and ALT (no. 41282, ALT) activities (Spinreact) were measured by spectrophotometry in a Multiskan GO spectrophotometer (Invitrogen-ThermoFisher). GDF15 serum levels were measured using mouse enzyme-linked immunosorbent assay kits (Cloud Clone Corp.). Serum cytokines (IL-6 and IP-10) were measured with a Milliplex kit (Millipore).

Real-time PCR analysis. For testis and adrenal gland analysis, real-time PCR (SYBR GreenER quantitative PCR SuperMix System; Invitrogen) was performed using the following specific primers:[57,58] STAR, forward 5′-AGTTCGACGTCGG AGCTCTCT-3′; reverse 5′-TACTTAGCACTTCGTCCCCG-3′; P450scc, forward 5′-GATTGCGGAGCTGGAGATGA-3′; reverse 5′-TCTTTTCTGGTCACGGC TGG-3′; 17β-HSD3, forward 5′-CTGAGCACTTCCGGTGAG AG-3′; reverse 5′-GGCCTTTCCTCCTTGACT CC-3′; luteinizing hormone β, forward 5′-GAGT TCTGCCCAGTCTGCAT-3′; reverse 5′-AGGAAAGGAGACTATGGGGTCT-3′ and S11 forward 5′-CATTCAGACGGAGCGTGCTTA C-3′; reverse 5′-TGCATC TTCATCTTCGTCAC-3′.

For the skeletal muscle thermogenic markers, RNA levels, real-time PCR (TaqMan, Applied Biosystems) was performed using the following primers: Atp2a2, forward 5′-TCCGCTACCTCATCTCATCC-3′; reverse 5′-CAGGTCTGG AGGATTGAACC-3′; Gdp2, forward 5′-GAAGGGGACTATTCTTGTGGGT-3′; reverse 5′-GGATGTCAAATTCGGGTGTGT-3′; Ppary, forward 5′-TCGCTGA TGCACTGCCTATG-3′; reverse 5′-GAGAGGTCCACAGAGCTGATT-3′; Ryr1, forward 5′-CAGTTTTTGCGGACGGATGAT-3′; reverse 5′-CACCGGCCTCC ACAGTATTG-3′; Sln, forward 5′-GAGGTGGAGAGACTGAGGTCCTTGG-3′; reverse 5′-GAAGCTCGGGGCACACAGCAG-3′ and Ucp3, forward 5′-GAGATG GTGACCTACGACATCA-3′; reverse 5′-GCGTTCATGTATCGGGTCTTTA-3′.

For the analysis of in vivo SF1-AMPKα1-DN expression, these primers were used: SF1-AMPKα1-DN, forward 5′-AAACACCAAGGCGTACGGAA-3′; reverse 5′-TGGCGGCCGCTCTAGATTAC-3′ and HPRT, forward 5′-GGTTAAGCAGTA CAGCCCCA-3′; reverse 5′-TCCAACACTTCGAGAGGTCC-3′.

AMPK activity assay. AMPK activity was measured with CycLex AMPK Kinase Assay (CY-1182, MBL International Corporation)[59,60]. Briefly, 10 µl of lysis buffer containing 5 µg of VMH protein was added to 90 µl of kinase assay buffer. Each sample was analysed in duplicate, and U2OS WT or AMPK KO cell extracts were used as controls. Absorbance was measured at 450/550 nm in a MultiSkan Go (Invitrogen).

Immunohistochemistry. Brains were postfixed overnight in 4% PFA at 4 °C, equilibrated in a solution containing 30% sucrose in Tris-buffered saline (TBS, pH 7.2) and sectioned into 30 µm coronal slices on a cryostat (CM3050S, Leica). Brain sections along the medial part of the medio-basal hypothalamus were selected. Brain slices were washed with TBS, blocked with SUMI solution (0.25% porcine gelatin and 0.5% Triton X-100 in TBS, pH 7.2) and incubated overnight at 4 °C with the following primary antibodies dissolved in SUMI solution: rabbit anti-pACCα-Ser^{79} (PA5-17725, Invitrogen-ThermoFisher), goat anti-GFAP (SAB2500462, Sigma-Aldrich) and goat anti-Iba1 (ab107519, Abcam). Brain slices were washed with TBS and incubated for 2 h at room temperature with the respective secondary antibodies diluted in SUMI: donkey antirabbit Alexa 647 (A21206, Invitrogen) and donkey antigoat Alexa 488 (A21206, Invitrogen). Sections were washed in TBS and incubated with 4,6-diamidino-2-phenylindole (DAPI) (D3571, Life Technologies) and/or NeuroTraceTM 500/525 (N21480, Invitrogen) in TBS. Images were acquired as *z* stacks using a confocal microscope (TCS SP8 Leica). ImageJ/FIJI was used to process the images. The quantifications were made on the basis of the visualization of cellular bodies using pACCα-Ser^{79} staining, which showed a predominant neuronal profiling. The presence and absence of pACCα-Ser^{79} in neurons within the VMH was assessed by using costaining with Neurotrace 500/525 (N21480, Invitrogen). No distinguished cellular staining of pACCα-Ser^{79} was discarded as part of the quantifications.

Double SF1 and pACCα-Ser^{79} immunofluorescence staining. Mice were anaesthetized and perfused with 0.9% saline solution followed by 4% PFA. Brains were removed, postfixed overnight in 4% PFA at 4 °C, washed with ice-cold 0.1 M PBS and transferred to 30% sucrose in 0.1 M PBS (pH 7.4) overnight at 4 °C, before being frozen at −80 °C. Sections 20-µm thick were obtained using a cryostat. Sections centred on the VMH were selected (−1.34 to −1.94 mm from Bregma) and processed for double immunofluorescence staining of SF1 neurons and pACCα-Ser^{79}. Briefly, the brain slices were washed with 0.1 M PBS three times for 5 min before being incubated with a blocking solution (5% normal donkey serum in 0.1 M PBS containing 0.3% Triton X-100) for 2 h at room temperature. Next, the slices were washed with 0.1 M PBS twice for 5 min and then incubated with the first primary antibody (SF1, 1:200 diluted in 0.1 M PBS; ab65815, Abcam) overnight at 4 C. Following three washes of 5 min in 0.1 M PBS, the slices were incubated with a donkey antirabbit Alexa Fluor 594 (1:1,000; A21207, Life Technologies) in 0.1 M PBS for 2 h at room temperature. As the two primary antibodies were obtained from rabbit, the brain sections were incubated with AffiniPure Fab Fragment goat antirabbit IgG (1:40; 111-007-003, Jackson ImmunoResearch) for 4 h at room temperature to saturate the remaining open binding sites on the first primary antibody to avoid any cross-reactivity between both antirabbit primary antibodies. After extensive washing, the slices were incubated with the second

primary antibody (pACCα-Ser[79], 1:100 diluted in 0.1 M PBS) overnight at 4 °C. The slices were then washed three times with 0.1 M PBS for 5 min before being incubated with a donkey antirabbit Alexa 488 (1:1,000; 711-545-512, Jackson ImmunoResearch) for 2 h at room temperature. Following a final step composed of three washes with 0.1 M PBS, slices were mounted using DAPI-containing Vectashield (Vector Laboratories) and stored in the dark at 4° C.

Images were acquired using a confocal Leica TCS SP-5-X microscope, equipped with a ×63 oil objective and using a zoom of ×3. Z-stacks of 1 µm of the VMH were captured bilaterally. To ensure similar imaging conditions for all pictures of VMH slices ($n = 3/4$ animals per group), exact same microscope setup (laser power and gain) was used to capture all pictures. Images were imported into FIJI (NIH), where maximum intensity projections were made and brightness and contrast were equally adjusted. For quantification, each SF1 positive neuron per section were manually selected and the intensity of pACC signal were analysed and are expressed as a percentage relative to control.

Western blotting. sEVs (10 µg) were separated on PAGE. After migration, proteins were transferred to nitrocellulose membranes and incubated with the following antibodies: Alix (Biolegend), CD9 (BD Pharmingen), CD81, TSG101 and GRP94 (Santa Cruz Biotechnology). To evaluate the transfection efficiency of the JAWS II cells with Lamp2b-RVG and its translocation to sEVs, purified sEVs (native or Lamp2b-RVG modified) were immunoblotted with Lamp2b (Abcam).

Protein lysates from tissues were subjected to SDS–PAGE, electrotransferred on a polyvinyl difluoride membrane and probed with the following antibodies: pACCα-Ser[79], ACCα (Cell Signalling), UCP1, UCP3, Lamp2b (Abcam), PGC1α, PGC1β, GRP94 (Santa Cruz Biotechnology), β-actin, α-tubulin (Sigma-Aldrich) and GAPDH (Millipore)[12,13,15–18,44]. Each membrane was then incubated with the corresponding secondary antibody: antimouse or antirabbit (DAKO). Values were expressed in relation to α-tubulin (for BAT, skeletal muscle and heart) or β-actin (for the rest of the analysed tissues) protein levels. Regarding sEVs, the values were expressed in relation to the total content of protein measured by Ponceau S. Autoradiographic films were scanned and the band signals were quantified by densitometry using ImageJ v.1.33 software (NIH).

Statistical analysis. Data are expressed as mean ± s.e.m.; when data are relativized, they are given as a percentage of the appropriate controls. Statistical significance was determined by two-sided (at least one-sided is specified) Student's *t*-test (when two groups were compared) or two-sided analysis of variance (ANOVA) (when more than two groups were compared) followed by a post hoc Bonferroni test. The relation between continuous variables was analysed by simple correlation (Pearson's test). $P < 0.05$ was considered significant. We carried out data analysis using GraphPad Instat and Prism Software (GraphPad).

Reporting Summary. Further information on research design is available in the Nature Research Reporting Summary linked to this article.

Data availability

All additional data that support the findings of this study are available from the corresponding authors (R.A. and M.L.) on request. Source data are provided with this paper.

Received: 30 October 2020; Accepted: 2 September 2021;

References

1. Clemmensen, C., Muller, T. D., Finan, B., Tschop, M. H. & DiMarchi, R. Current and emerging treatment options in diabetes care. *Handb. Exp. Pharmacol.* **233**, 437–459 (2016).
2. Tschop, M. H. et al. Unimolecular polypharmacy for treatment of diabetes and obesity. *Cell Metab.* **24**, 51–62 (2016).
3. López, M., Nogueiras, R., Tena-Sempere, M. & Dieguez, C. Hypothalamic AMPK: a canonical regulator of whole-body energy balance. *Nat. Rev. Endocrinol.* **12**, 421–432 (2016).
4. Cui, H., López, M. & Rahmouni, K. The cellular and molecular bases of leptin and ghrelin resistance in obesity. *Nat. Rev. Endocrinol.* **13**, 338–351 (2017).
5. Muller, T. D., Clemmensen, C., Finan, B., Dimarchi, R. D. & Tschop, M. H. Anti-obesity therapy: from rainbow pills to polyagonists. *Pharmacol. Rev.* **70**, 712–746 (2018).
6. Dragano, N. R. V., Ferno, J., Dieguez, C., Lopez, M. & Milbank, E. Recent updates on obesity treatments: available drugs and future directions.*Neuroscience* **437**, 215–239 (2020).
7. Kahn, B. B., Alquier, T., Carling, D. & Hardie, D. G. AMP-activated protein kinase: ancient energy gauge provides clues to modern understanding of metabolism. *Cell Metab.* **1**, 15–25 (2005).
8. Schneeberger, M. & Claret, M. Recent insights into the role of hypothalamic AMPK signaling cascade upon metabolic control. *Front Neurosci.* **6**, 185 (2012).
9. Hardie, D. G., Schaffer, B. E. & Brunet, A. AMPK: an energy-sensing pathway with multiple inputs and outputs.*Trends Cell Biol.* **26**, 190–201 (2015).
10. Carling, D. AMPK signalling in health and disease. *Curr. Opin. Cell Biol.* **45**, 31–37 (2017).
11. Lopez, M. AMPK wars: the VMH strikes back, return of the PVH. *Trends Endocrinol. Metab.* **29**, 135–137 (2018).
12. López, M. et al. Hypothalamic AMPK and fatty acid metabolism mediate thyroid regulation of energy balance. *Nat. Med.* **16**, 1001–1008 (2010).
13. Martínez de Morentin, P. B. et al. Nicotine induces negative energy balance through hypothalamic AMP-activated protein kinase. *Diabetes* **61**, 807–817 (2012).
14. Whittle, A. J. et al. Bmp8b increases brown adipose tissue thermogenesis through both central and peripheral actions. *Cell* **149**, 871–885 (2012).
15. Martínez de Morentin, P. B. et al. Estradiol regulates brown adipose tissue thermogenesis via hypothalamic AMPK. *Cell Metab.* **20**, 41–53 (2014).
16. Martins, L. et al. A functional link between AMPK and orexin mediates the effect of BMP8B on energy balance. *Cell Rep.* **16**, 2231–2242 (2016).
17. Martínez-Sánchez, N. et al. Hypothalamic AMPK-ER stress-JNK1 axis mediates the central actions of thyroid hormones on energy balance. *Cell Metab.* **26**, 212–229 (2017).
18. Seoane-Collazo, P. et al. SF1-specific AMPKalpha1 deletion protects against diet-induced obesity. *Diabetes* **67**, 2213–2226 (2018).
19. Buzas, E. I., Gyorgy, B., Nagy, G., Falus, A. & Gay, S. Emerging role of extracellular vesicles in inflammatory diseases. *Nat. Rev. Rheumatol.* **10**, 356–364 (2014).
20. Milbank, E., Martinez, M. C. & Andriantsitohaina, R. Extracellular vesicles: pharmacological modulators of the peripheral and central signals governing obesity. *Pharmacol. Ther.* **157**, 65–83 (2016).
21. Martinez, M. C. & Andriantsitohaina, R. Extracellular vesicles in metabolic syndrome. *Circ. Res.* **120**, 1674–1686 (2017).
22. Malloci, M. et al. Extracellular vesicles: mechanisms in human health and disease. *Antioxid. Redox Signal* **30**, 813–856 (2019).
23. López, M. et al. Hypothalamic fatty acid metabolism mediates the orexigenic action of ghrelin. *Cell Metab.* **7**, 389–399 (2008).
24. Tang, K. et al. Delivery of chemotherapeutic drugs in tumour cell-derived microparticles. *Nat. Commun.* **3**, 1282 (2012).
25. Dalli, J. et al. Microparticle alpha-2-macroglobulin enhances pro-resolving responses and promotes survival in sepsis. *EMBO Mol. Med.* **6**, 27–42 (2014).
26. Kamerkar, S. et al. Exosomes facilitate therapeutic targeting of oncogenic KRAS in pancreatic cancer. *Nature* **546**, 498–503 (2017).
27. Quah, B. J. & O'Neill, H. C. The immunogenicity of dendritic cell-derived exosomes. *Blood Cells Mol. Dis.* **35**, 94–110 (2005).
28. Alvarez-Erviti, L. et al. Delivery of siRNA to the mouse brain by systemic injection of targeted exosomes. *Nat. Biotechnol.* **29**, 341–345 (2011).
29. Colombo, M., Raposo, G. & Thery, C. Biogenesis, secretion, and intercellular interactions of exosomes and other extracellular vesicles. *Annu. Rev. Cell Dev. Biol.* **30**, 255–289 (2014).
30. Kumar, P. et al. Transvascular delivery of small interfering RNA to the central nervous system. *Nature* **448**, 39–43 (2007).
31. Domingos, R. F. et al. Characterizing manufactured nanoparticles in the environment: multimethod determination of particle sizes. *Environ. Sci. Technol.* **43**, 7277–7284 (2009).
32. Parker, K. L. & Schimmer, B. P. Steroidogenic factor 1: a key determinant of endocrine development and function. *Endocr. Rev.* **18**, 361–377 (1997).
33. Choi, Y. H., Fujikawa, T., Lee, J., Reuter, A. & Kim, K. W. Revisiting the ventral medial nucleus of the hypothalamus: the roles of SF-1 neurons in energy homeostasis. *Front Neurosci.* **7**, 71 (2013).
34. Corley, D. R., Li, X., Lei, Z. M. & Rao, C. V. Potential regulation of GnRH gene by a steroidogenic factor-1-like protein. *Mol. Hum. Reprod.* **6**, 671–676 (2000).
35. Mellon, P. L. et al. Immortalization of hypothalamic GnRH neurons by genetically targeted tumorigenesis. *Neuron* **5**, 1–10 (1990).
36. Coyral-Castel, S. et al. The effect of AMP-activated kinase activation on gonadotrophin-releasing hormone secretion in GT1-7 cells and its potential role in hypothalamic regulation of the oestrous cyclicity in rats. *J. Neuroendocrinol.* **20**, 335–346 (2008).
37. Beall, C. et al. Mouse hypothalamic GT1-7 cells demonstrate AMPK-dependent intrinsic glucose-sensing behaviour. *Diabetologia* **55**, 2432–2444 (2012).
38. Schimmer, B. P. & White, P. C. Minireview: steroidogenic factor 1: its roles in differentiation, development, and disease. *Mol. Endocrinol.* **24**, 1322–1337 (2010).
39. Warner, A. et al. Inappropriate heat dissipation ignites brown fat thermogenesis in mice with a mutant thyroid hormone receptor alpha1. *Proc. Natl Acad. Sci. USA* **110**, 16241–16246 (2013).
40. Yang, Q. et al. AMPK/alpha-ketoglutarate axis dynamically mediates DNA demethylation in the Prdm16 promoter and brown adipogenesis. *Cell Metab.* **24**, 542–554 (2016).

41. Cannon, B. & Nedergaard, J. Brown adipose tissue: function and physiological significance. *Physiol. Rev.* **84**, 277–359 (2004).
42. Morrison, S. F., Madden, C. J. & Tupone, D. Central neural regulation of brown adipose tissue thermogenesis and energy expenditure. *Cell Metab.* **19**, 741–756 (2014).
43. Contreras, C. et al. The brain and brown fat. *Ann. Med* **47**, 150–168 (2015).
44. Gonzalez-Garcia, I. et al. Estradiol regulates energy balance by ameliorating hypothalamic ceramide-induce ER stress. *Cell Rep.* **25**, 413–423 (2018).
45. Alvarez-Crespo, M. et al. Essential role of UCP1 modulating the central effects of thyroid hormones on energy balance. *Mol. Metab.* **5**, 271–282 (2016).
46. Claret, M. et al. AMPK is essential for energy homeostasis regulation and glucose sensing by POMC and AgRP neurons. *J. Clin. Invest.* **117**, 2325–2336 (2007).
47. Foretz, M., Guigas, B., Bertrand, L., Pollak, M. & Viollet, B. Metformin: from mechanisms of action to therapies. *Cell Metab.* **20**, 953–966 (2014).
48. Foretz, M. & Viollet, B. Therapy: metformin takes a new route to clinical efficacy. *Nat. Rev. Endocrinol.* **11**, 390–392 (2015).
49. Campderros, L. et al. Brown adipocytes secrete GDF15 in response to thermogenic activation. *Obes. (Silver Spring)* **27**, 1606–1616 (2019).
50. Johann, K. et al. Thyroid-hormone-induced browning of white adipose tissue does not contribute to thermogenesis and glucose consumption. *Cell Rep.* **27**, 3385–3400 e3383 (2019).
51. Seoane-Collazo, P. et al. Central nicotine induces browning through hypothalamic kappa opioid receptor. *Nat. Commun.* **10**, 4037 (2019).
52. Johnson, D. H., Flask, C. A., Ernsberger, P. R., Wong, W. C. & Wilson, D. L. Reproducible MRI measurement of adipose tissue volumes in genetic and dietary rodent obesity models. *J. Magn. Reson. Imaging* **28**, 915–927 (2008).
53. Hu, H. H., Chen, J. & Shen, W. Segmentation and quantification of adipose tissue by magnetic resonance imaging. *MAGMA* **29**, 259–276 (2016).
54. Hong, C. W., Fazeli Dehkordy, S., Hooker, J. C., Hamilton, G. & Sirlin, C. B. Fat quantification in the abdomen. *Top. Magn. Reson Imaging* **26**, 221–227 (2017).
55. Contreras, C. & Lopez, M. Ceramide sensing in the hippocampus: the lipostatic theory and Ockham's razor. *Mol. Metab.* **3**, 90–91 (2014).
56. Heras, V. et al. Central ceramide signaling mediates obesity-induced precocious puberty. *Cell Metab.* **32**, 951–966 e958 (2020).
57. Vazquez, M. J. et al. SIRT1 mediates obesity- and nutrient-dependent perturbation of pubertal timing by epigenetically controlling Kiss1 expression. *Nat. Commun.* **9**, 4194 (2018).
58. Sanchez-Garrido, M. A. et al. Intergenerational influence of paternal obesity on metabolic and reproductive health parameters of the offspring: male-preferential impact and involvement of Kiss1-mediated pathways. *Endocrinology* **159**, 1005–1018 (2018).
59. Zadra, G. et al. A novel direct activator of AMPK inhibits prostate cancer growth by blocking lipogenesis. *EMBO Mol. Med.* **6**, 519–538 (2014).
60. Tang, Y. C., Williams, B. R., Siegel, J. J. & Amon, A. Identification of aneuploidy-selective antiproliferation compounds. *Cell* **144**, 499–512 (2011).

Acknowledgements

The research leading to these results has received funding from the Xunta de Galicia (R.N. grant no. 2016-PG057, M.L. grant no. 2016-PG068); EuroNanoMed III (R.A. and M.L. grant no. EURONANOMED2019-050/ENAMEP); Junta de Andalucía (M.T.-S. grant no. P12-FQM-01943); Ministerio de Ciencia y Universidades cofunded by the FEDER Program of EU (C.D. grant no. BFU2017-87721; M.T.-S. grant no. BFU2014-57581-P, R.N. grant no. BFU2015-70664R; M.L. grant no. RTI2018–101840-B-I00 and grant no. BFU2015-70454-REDT/Adipoplast); USA National Institutes of Health (K.R. grant no. HL084207); the German Research Foundation (DFG) (grant nos. MI1242/3-2 to J.M. and OE723/2-1 to R.O.); the USA Department of Veterans Affairs (K.R. grant no. I01BX004249); The University of Iowa Fraternal Order of Eagles Diabetes Research Center (K.R.); European Research Council ERC (C.G.-C. STG grant AstroNeuroCrosstalk no. 757393); Atresmedia Corporación (R.N. and M.L. grant no. 2017-PO004) and 'la Caixa' Foundation (grant no. ID 100010434), under grant agreement no. LCF/PR/HR19/52160022 (M.L.). E.M. was recipient of a Predoctoral Fellowship of the Nanofar Erasmus Mundus Program. I.G.-G. is recipient of a fellowship from Alexander von Humboldt Foundation (ref. 3.3, ESP-1206916-HFST-P) and European Union's Horizon 2020 research and innovation programme under the Marie Sklodowska-Curie actions (grant no. 842080, H2020-MSCA-IF-2018). T.S. is recipient of a research contract from the Miguel Servet Program (CPII17/00027, Instituto de Salud Carlos III). The CiM USA is supported by the Xunta de Galicia (grant no. 2016-2019, ED431G/05). CIBER de Fisiopatología de la Obesidad y Nutrición is an initiative of ISCIII. INSERM U1063 is supported by the Institut National de Santé et Recherche Médicale and Université d'Angers. The funders had no role in study design, data collection and analysis, decision to publish or preparation of the paper. We thank S. Recoquillon and M. Wertheimer for technical assistance. The TEM analysis was performed in the Service Commun d'Imageries et d'Analyses Microscopiques of University of Angers. We thank SCAHU staff (Université d'Angers) for taking care of animals. The PET–CT analysis was performed in the Molecular Imaging Unit of the Department of Nuclear Medicine of USC. Q12

Author contributions

E.M., N.R.V.D., I.G.-G., M.R.-G., F.R.-P., V.R.-L., C.C., J.C. and B.P. performed the in vivo experiments, analytical methods and collected and analysed the data. E.M., L.P., G.H., P.M. and L.V. generated and validated the sEVs. F.R.-P., J.R. and M.T.-S. analysed testis and adrenal function. D.A.M. and K.R. performed and analysed the SNA studies. R.I.-R. and T.S. performed the NMR studies. A.G.-N. and F.V. performed the experiments with brown adipocytes. N.R.V.D., I.G.-G. and C.G.-C. performed the immunohistochemistry studies. R.O. and J.M. provided the ucp1 null mice. E.M., N.R.V.D., I.G.-G., A.V., F.V., C.D., R.N., C.G.-C., M.T.-S., M.C.M., J.M., K.R., R.A. and M.L. analysed, interpreted and discussed the data. E.M., M.C.M., R.A. and M.L. developed the hypothesis and conceived and designed the experiments. E.M. and M.L. made the figures and wrote the paper. All authors revised and edited the paper. R.A. and M.L. jointly supervised this work, secured funding, coordinated the project and served as guarantors. M.L. is the lead contact for this study.

Competing interests

E.M., M.C.M., R.A. and M.L. declare that the research described in this paper is patent pending: European Patent Application EP21382763.7 entitled 'Populations of small extracellular vesicles for use in the treatment of obesity', European Patent Office (EPO). The other authors declare no competing interests. Q14

Additional information

Extended data are available for this paper at https://doi.org/10.1038/s42255-021-00467-8.

Supplementary information The online version contains supplementary material available at https://doi.org/10.1038/s42255-021-00467-8.

Correspondence and requests for materials should be addressed to Ramaroson Andriantsitohaina or Miguel López.

Peer review information *Nature Metabolism* thanks Christopher Madden and the other, anonymous, reviewer(s) for their contribution to the peer review of this work. Primary Handling Editor: Christoph Schmitt.

Reprints and permissions information is available at www.nature.com/reprints.

Publisher's note Springer Nature remains neutral with regard to jurisdictional claims in published maps and institutional affiliations.

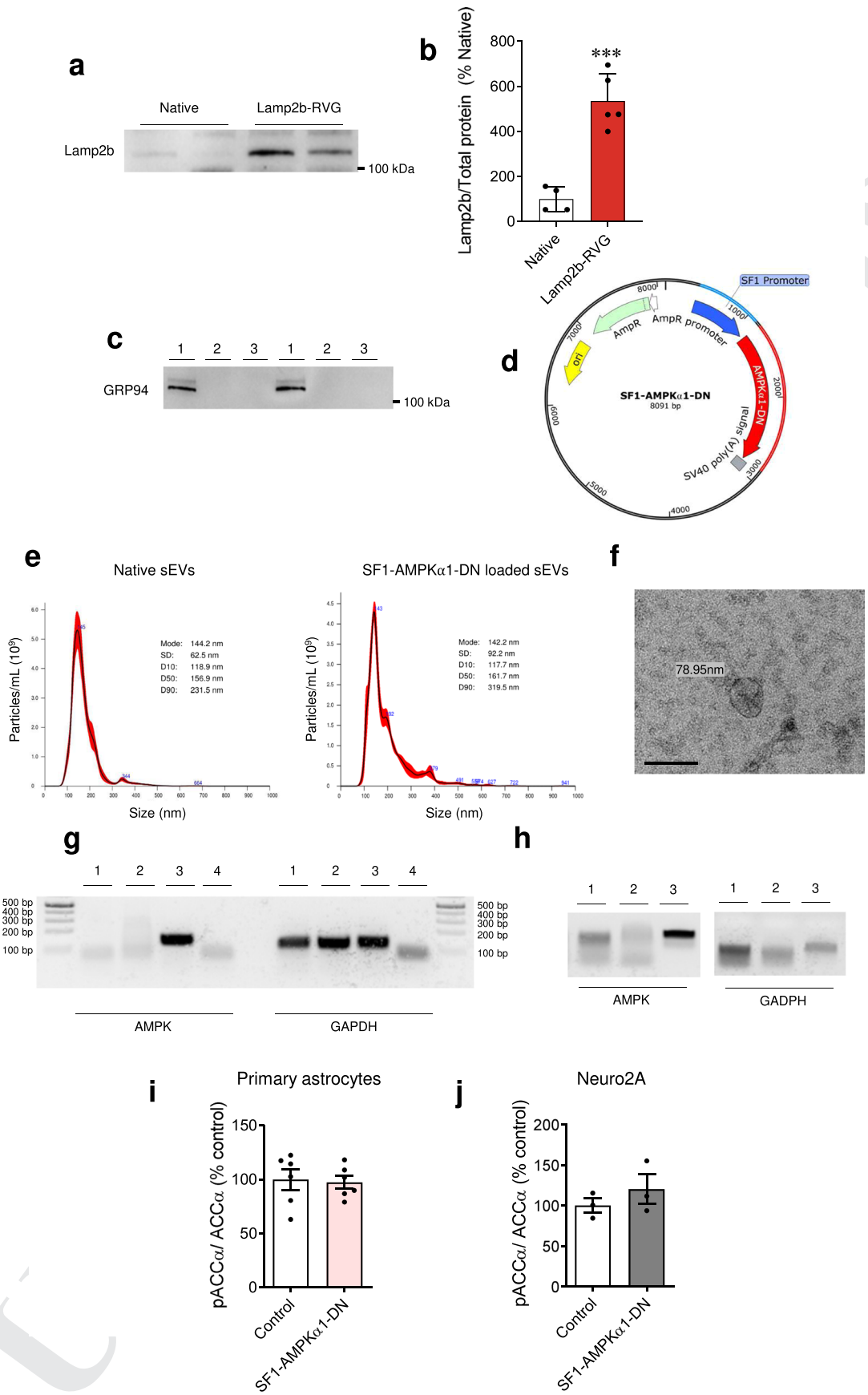

Extended Data Fig. 1 | See next page for caption.

Extended Data Fig. 1 | Characterization of SF1-AMPKα1-DN loaded neuronal-targeted dendritic cell-derived sEVs. a, Western blotting using antibodies against Lamp2b in native and Lamp2b-RVG sEVs. **b**, Quantification of Lamp2b levels in native (n = 4 samples) and Lamp2b-RVG (n = 5 samples) sEVs in % of native control; P = 0.00031. **c**, Western blotting using antibodies against GRP94 in Jaws II cells (lane 1), unmodified native sEVs (lane 2) and Lamp2b-RVG sEVs (lane 3). **d**, Circular representation of the SF1-AMPKα1-DN encoding plasmid. **e**, Example of curve obtained by nanoparticle tracking analysis of a sample of native (left panel) and SF1-AMPKα1-DN loaded Lamp2b-RVG sEVs (right panel). The graph represents concentration of sEVs (particles/mL) according to the size (nm). **f**, Electron microscopy image of SF1-AMPKα1-DN loaded Lamp2b-RVG sEVs showing specific round shape and average size of ~70 nm vesicles. **g**, Agarose gel electrophoresis of native (lane 1), Lamp2b-RVG (lane 2), SF1-AMPKα1-DN loaded Lamp2b-RVG sEVs (lane 3) and negative control H2O (lane 4) of AMPK and GAPDH. **h**, Agarose gel electrophoresis of SF1-AMPKα1-DN loaded Lamp2b-RVG sEVs treated with DNAse (lane 1), DNAse + Triton X-100 0.2% (lane 2) and Triton X-100 0.2% (lane 3) of AMPK and GAPDH. **i**, Quantification of pACCα/ACCα in primary astrocytes treated for 24 h with native and Lamp2b-RVG (n = 6 samples/group) sEVs. **j**, Quantification of pACCα/ACCα in Neuro2A cells treated for 24 h with native and Lamp2b-RVG (n = 3 samples per group) sEVs. Data expressed as mean ± SEM. ***P < 0.001 vs. Control. Statistical significance was assessed by two-sided Student's t-test.

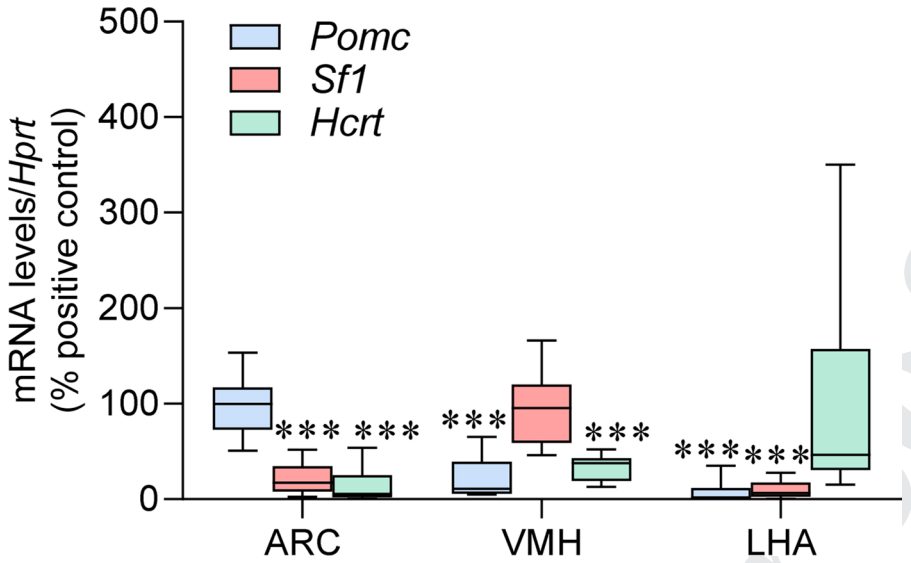

Extended Data Fig. 2 | Control of hypothalamic nuclei dissections. Quantification of Pomc, Sf1 and Hcrt/orexin mRNA levels in ARC, VMH and LHA dissections [Pomc: ARC n = 20 mice, VMH n = 20 mice, LHA n = 19 mice; Sf1: ARC n = 19 mice, VMH n = 19 mice, LHA n = 19 mice; Hcrt: ARC n = 20 mice, VMH n = 20 mice, LHA n = 19 mice; box plots indicate median (middle line), 25th, 75th percentile (box) and 10th-90th percentiles (whiskers; minima and maxima, respectively)]. Data expressed as mean ± SEM. ***$P < 0.001$ vs. Pomc ARC, Sf1 VMH and Hcrt LHA. Statistical significance was assessed by two-sided ANOVA.

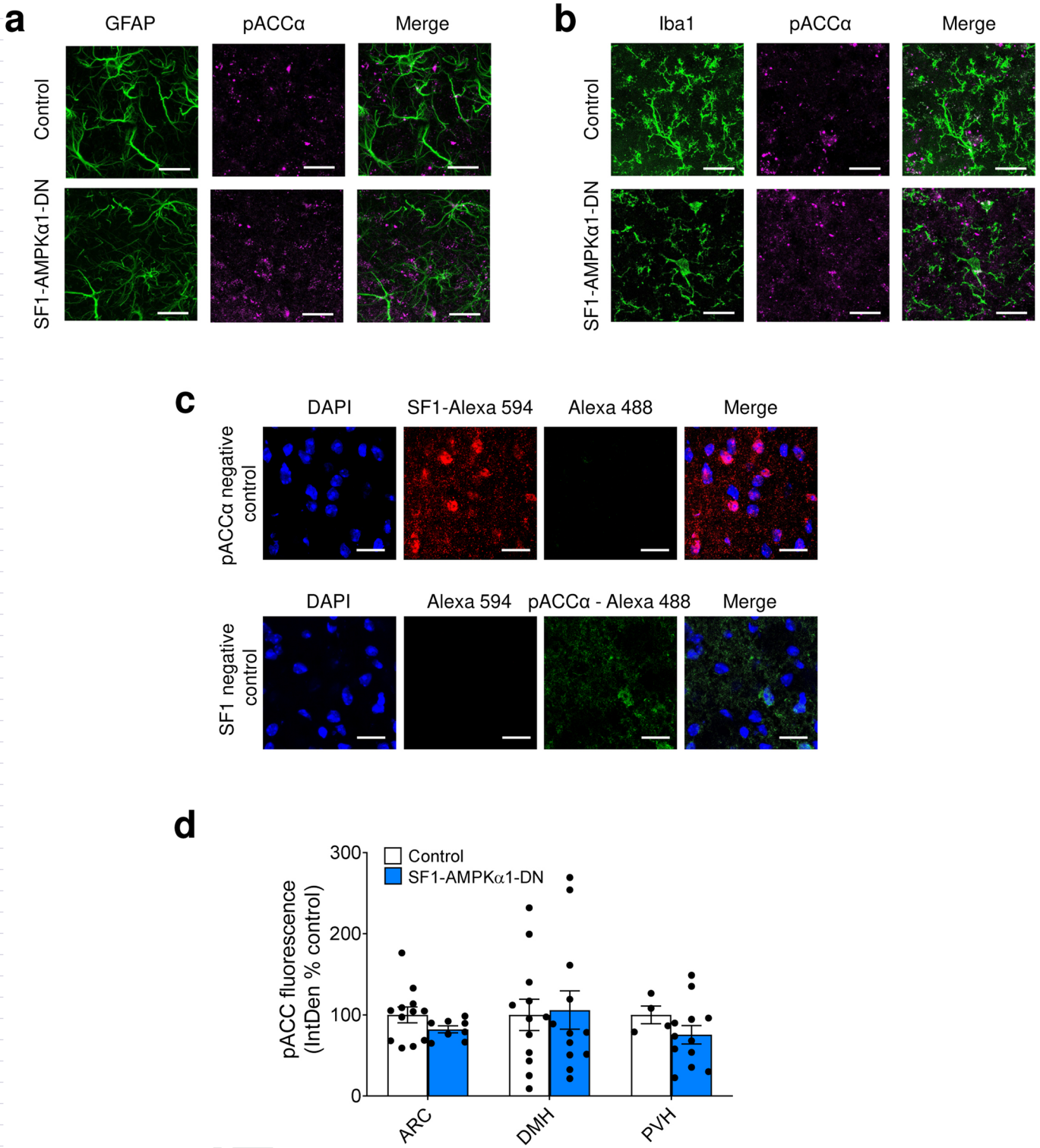

Extended Data Fig. 3 | Effect of systemic treatment with SF1-AMPKα1-DN loaded sEVs on hypothalamic AMPK activity in DIO mice. a, Representative confocal images depicting GFAP (green), pACCα (magenta) and merged reactivity in brain sections (control n = 8 fields, 4 mice/group; SF1-AMPKα1-DN n = 8 fields, 4 mice/group) after 24 h of intravenous injection with control (non-loaded) or SF1-AMPKα1-DN loaded sEVs; scale bars represent 20 µm. **b**, Representative confocal images depicting Iba1 (green), pACCα (magenta) and merged reactivity in brain sections after 24 h of intravenous injection with control (non-loaded) or SF1-AMPKα1-DN loaded sEVs; scale bars represent 20 µm. **c**, Negative controls for pACCα and SF1 double immunofluorescence. Representative confocal images depicting DAPI (blue), Alexa594, with or without SF1 (red), Alexa 488 with or without pACCα (green) and merged reactivity in brain sections; scale bars represent 20 µm. The experiments were repeated 3 times. **d**, Quantification of pACCα fluorescence in ARC, DMH and PVH (quantification per field; ARC control n = 12 fields, 3 mice/group; SF1-AMPKα1-DN n = 8 fields, 2 mice/group; DMH control n = 12 fields, 3 mice/group; SF1-AMPKα1-DN n = 12 fields, 3 mice/group; PVH control n = 4 fields, 1 mice/group; SF1-AMPKα1-DN n = 12 fields, 3 mice/group) after 24 h of intravenous injection with control (non-loaded) or SF1-AMPKα1-DN loaded sEVs. Data expressed as mean ± SEM. Statistical significance was assessed by two-sided Student's t-test.

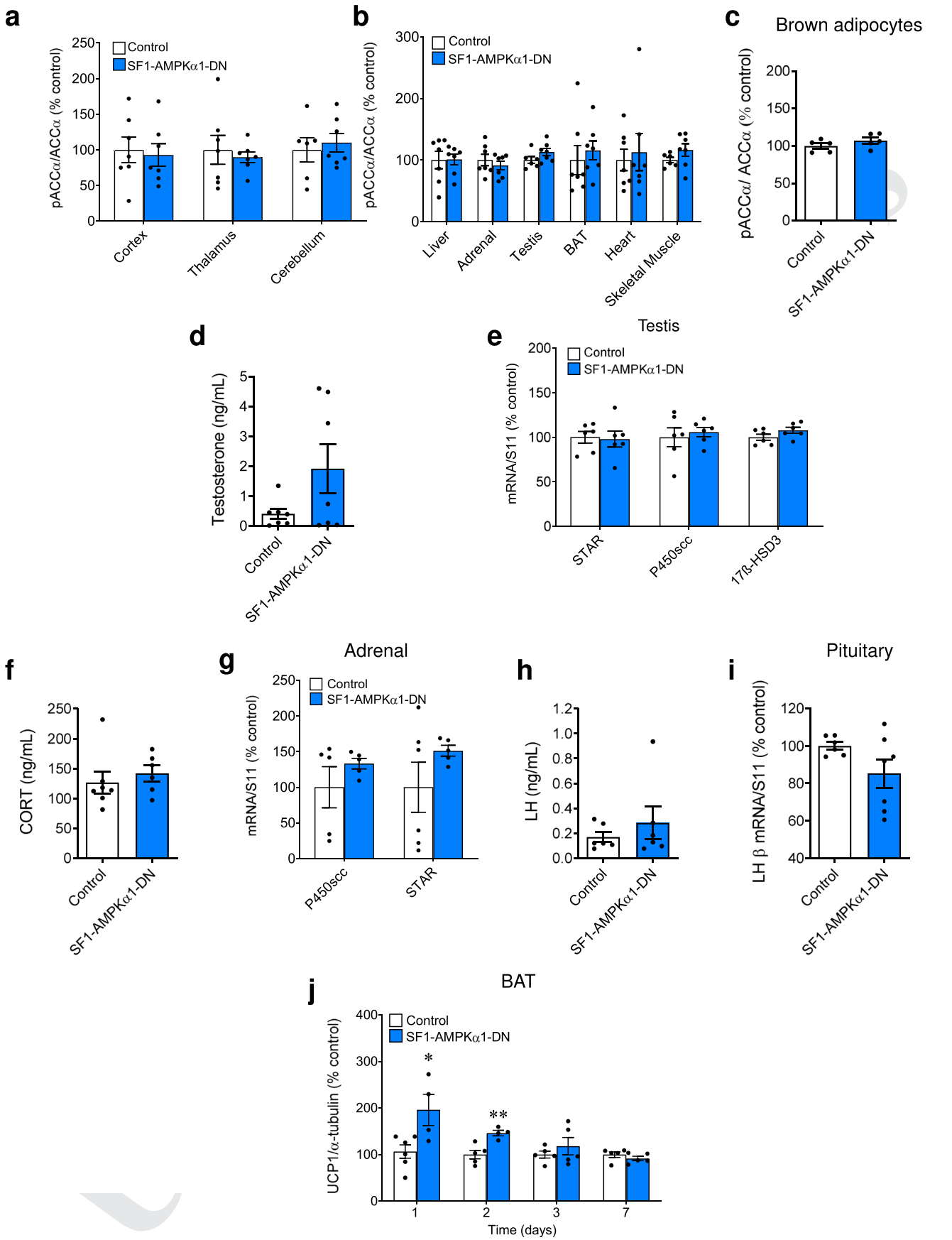

Extended Data Fig. 4 | See next page for caption.

Extended Data Fig. 4 | Effect of systemic treatment with SF1-AMPKα1-DN loaded sEVs on central and peripheral tissues in DIO mice. a, Quantification of pACCα/ACCα levels in cortex, thalamus and cerebellum after 28-day of intravenous injection with control (non-loaded; cortex n = 7 mice; thalamus n = 7 mice; cerebellum n = 6 mice) or SF1-AMPKα1-DN loaded (cortex n = 7 mice; thalamus n = 7 mice; cerebellum n = 7 mice) sEVs. **b**, Quantification of pACCα/ACCα levels in liver, adrenal gland, testis, BAT, heart and skeletal muscle after 28-day of intravenous injection with control (non-loaded, liver n = 7 mice; adrenal n = 7 mice; testis n = 6 mice; BAT n = 7 mice; heart n = 7 mice; skeletal muscle n = 6 mice) or SF1-AMPKα1-DN loaded (liver n = 7 mice; adrenal n = 7 mice; testis n = 7 mice; BAT n = 7 mice; heart n = 7 mice; skeletal muscle n = 7 mice) sEVs. **c**, Quantification of pACCα/ACCα levels in brown adipocytes after 24 h of incubation with control (non-loaded) or SF1-AMPKα1-DN loaded (n = 5 samples/group) sEVs. **d**, Quantification of circulating testosterone levels after 28-day of intravenous injection with control (non-loaded) or SF1-AMPKα1-DN loaded (n = 7 mice/group) sEVs. **e**, Quantification of mRNA levels of steroidogenic enzymes (STAR, p450scc and 17β-HSD3) in testis after 28-day of intravenous injection with control (non-loaded) or SF1-AMPKα1-DN loaded (n = 7 mice/group) sEVs. **f**, Quantification of circulating CORT levels after 28-day of intravenous injection with control (non-loaded, n = 7 mice) or SF1-AMPKα1-DN loaded (n = 6 mice) sEVs. **g**, Quantification of mRNA levels of P450scc and STAR in adrenals after 28-day of intravenous injection with control (non-loaded; P450scc n = 5 mice; STAR n = 6 mice) or SF1-AMPKα1-DN loaded (P450scc n = 5 mice/group; STAR n = 5 mice/group) sEVs. **h**, Quantification of circulating LH levels after 28-day of intravenous injection with control (non-loaded) or SF1-AMPKα1-DN loaded (n = 6 mice/group) sEVs. **i**, Quantification of mRNA levels of LH β subunit in pituitary after 28-day of intravenous injection with control (non-loaded, n = 6 mice) or SF1-AMPKα1-DN loaded (n = 7 mice) sEVs. **a**-**i**, **j**, Quantification of BAT UCP1 levels at 1, 2, 3 and 7 days after a single injection in the tail vein of control (non-loaded; day 1 n = 6 mice; day 2 n = 5 mice; day 3 n = 5 mice; day 7 n = 5 mice) or SF1-AMPKα1-DN sEVs (day 1 n = 4 mice; day 2 n = 4 mice; day 3 n = 5 mice; day 7 n = 5 mice) at day 0; day 1 $P = 0.023$; day 2 $P = 0.0054$. Data expressed as mean ± SEM. *$P < 0.05$ and **$P < 0.01$ vs. Control. Statistical significance was assessed by two-sided Student's t-test.

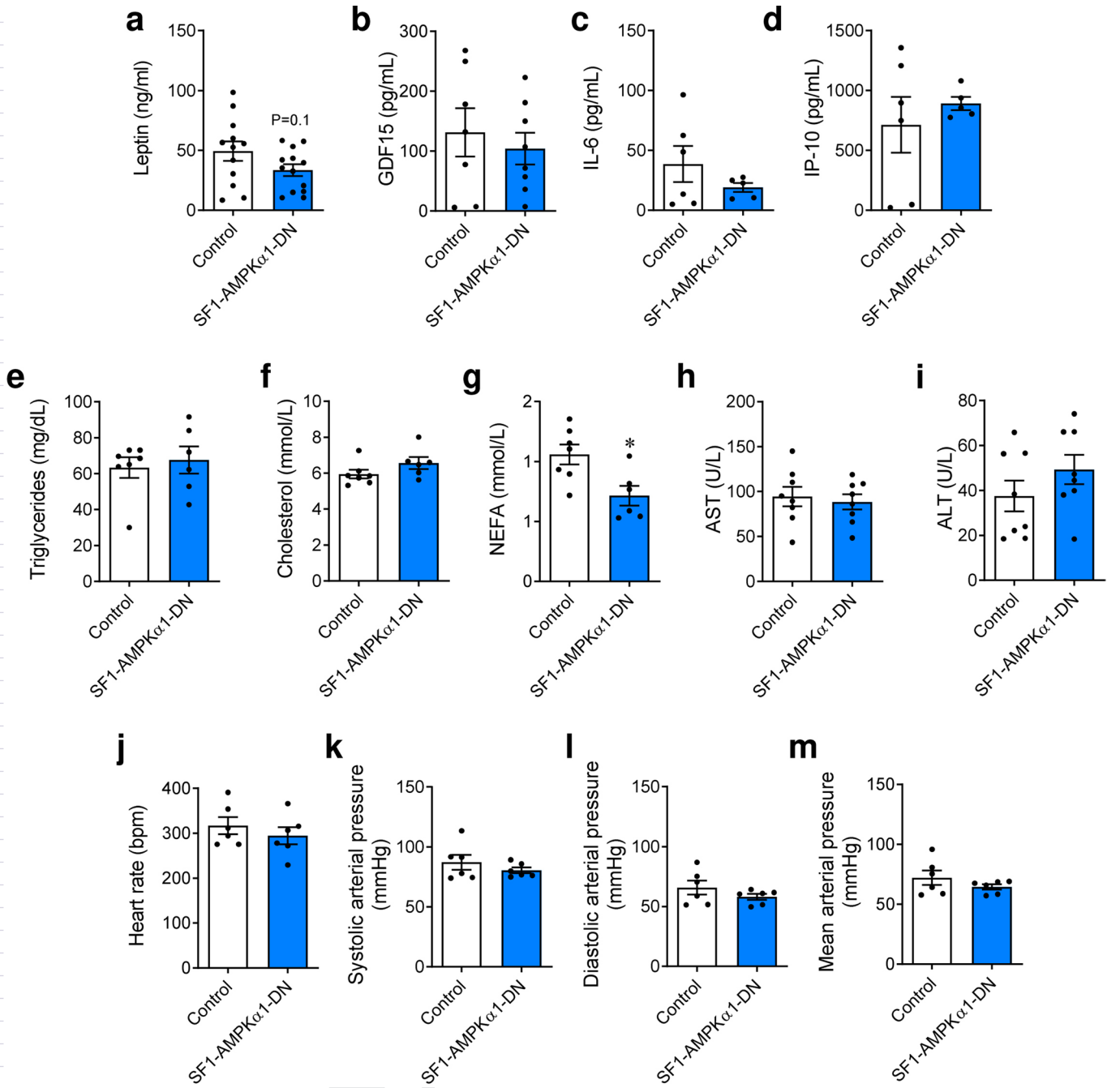

Extended Data Fig. 5 | Effect of systemic treatment with SF1-AMPKα1-DN sEVs on circulating and hemodynamic parameters in DIO mice. a-i, Quantification of circulating leptin (a; control n = 12 mice, SF1-AMPKα1-DN n = 13 mice), GDF15 (b; control n = 7 mice, SF1-AMPKα1-DN n = 8 mice), IL-6 (c; control n = 6 mice, SF1-AMPKα1-DN n = 5 mice), IP-10 (d; control n = 6 mice, SF1-AMPKα1-DN n = 5 mice), triglycerides (e; control n = 7 mice, SF1-AMPKα1-DN n = 6 mice), cholesterol (f; control n = 7 mice, SF1-AMPKα1-DN n = 6 mice), NEFA (g; control n = 7 mice, SF1-AMPKα1-DN n = 6 mice, P = 0,0142), AST (h; control n = 8 mice, SF1-AMPKα1-DN n = 8 mice) and ALT (i; control n = 8 mice, SF1-AMPKα1-DN n = 8 mice) after 28-day of intravenous injection with control (non-loaded) or SF1-AMPKα1-DN loaded sEVs. **j-m**, Quantification of heart rate (j, control n = 6 mice, SF1-AMPKα1-DN n = 6 mice), systolic arterial pressure (k; control n = 6 mice, SF1-AMPKα1-DN n = 6 mice), diastolic arterial pressure (l; n control n = 6 mice, SF1-AMPKα1-DN n = 6 mice) and mean arterial pressure (m; n = 6 mice/group) after 24 h of intravenous injection with control (non-loaded) or SF1-AMPKα1-DN loaded sEVs. Data expressed as mean ± SEM. Statistical significance was assessed by two-sided Student's t-test.

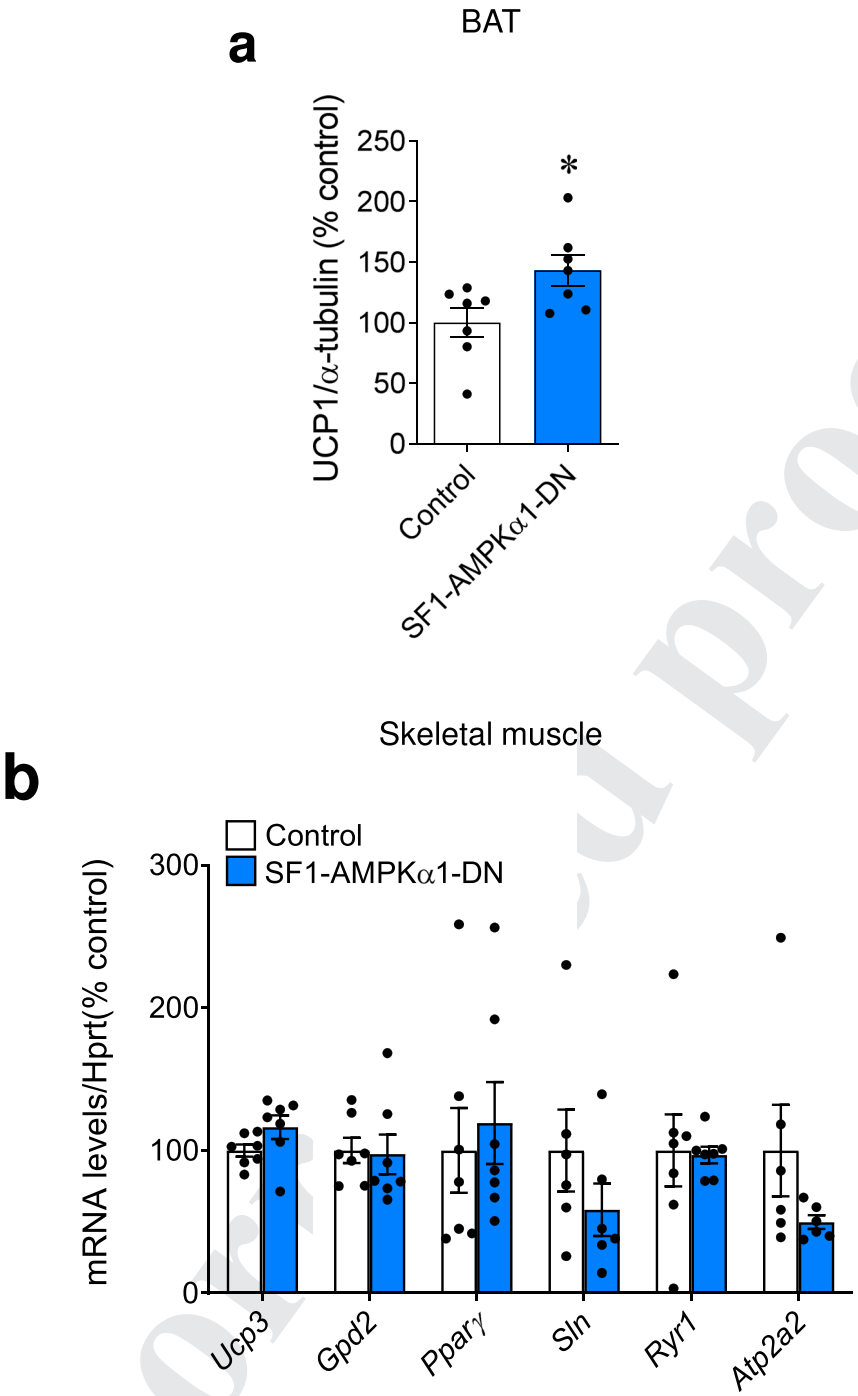

Extended Data Fig. 6 | Effect of systemic treatment with SF1-AMPKα 1-DN sEVs on BAT and skeletal muscle thermogenic markers in DIO mice. a, Quantification of UCP1 protein levels in the BAT after 28-day of intravenous injection with control (non-loaded) or SF1-AMPKα1-DN loaded (n = 7 mice/group) sEVs; P = 0.029. **b**, Quantification of mRNA levels of thermogenic markers (Ucp3, Gpd2, Pparɣ, Sln, Ryr1, Atp2a2) in skeletal muscle after 28-day of intravenous injection with control (non-loaded; Ucp3 n = 7 mice; Gpd2 n = 7 mice; Pparγ n = 7 mice; Sln n = 6 mice; Ryr n = 7 mice; Atp2a2 n = 6 mice) or SF1-AMPKα1-DN loaded (Ucp3 n = 7 mice; Gpd2 n = 7 mice; Pparγ n = 7 mice; Sln n = 6 mice; Ryr n = 7 mice; Atp2a2 n = 6 mice) sEVs. Data expressed as mean ± SEM. *, **P < 0.05 vs. Control. Statistical significance was assessed by two-sided Student´s t-test.

QUERY FORM

Nature Metabolism	
Manuscript ID	**[Art. Id: 467]**
Author	**Edward Milbank**

AUTHOR:

The following queries have arisen during the editing of your manuscript. Please answer by making the requisite corrections directly in the e.proofing tool rather than marking them up on the PDF. This will ensure that your corrections are incorporated accurately and that your paper is published as quickly as possible.

Query No.	*Nature of Query*
Q1:	Please check your article carefully, coordinate with any co-authors and enter all final edits clearly in the eproof, remembering to save frequently. Once corrections are submitted, we cannot routinely make further changes to the article.
Q2:	Note that the eproof should be amended in only one browser window at any one time; otherwise changes will be overwritten.
Q3:	Author surnames have been highlighted. Please check these carefully and adjust if the first name or surname is marked up incorrectly. Note that changes here will affect indexing of your article in public repositories such as PubMed. Also, carefully check the spelling and numbering of all author names and affiliations, and the corresponding email address(es).
Q4:	You cannot alter accepted Supplementary Information files except for critical changes to scientific content. If you do resupply any files, please also provide a brief (but complete) list of changes. If these are not considered scientific changes, any altered Supplementary files will not be used, only the originally accepted version will be published.
Q5:	If applicable, please ensure that any accession codes and datasets whose DOIs or other identifiers are mentioned in the paper are scheduled for public release as soon as possible, we recommend within a few days of submitting your proof, and update the database record with publication details from this article once available.
Q6:	Your paper has been copy edited. Please review every sentence to ensure that it conveys your intended meaning; if changes are required, please provide further clarification rather than reverting to the original text. Please note that formatting (including hyphenation, Latin words, and any reference citations that might be mistaken for exponents) has been made consistent with our house style.
Q7:	Please ensure that genes are correctly distinguished from gene products: for genes, official gene symbols (e.g., NCBI Gene) for the relevant species should be used and italicized; gene products such as proteins and noncoding RNAs should not be italicized.
Q8:	Please note, we reserve 'significant' and its derivatives for statistical significance. Please reword where this is not the intended meaning (for example to important, notable, substantial); there are 30 instances throughout your text.
Q9:	Please add individual descriptions to the caption to Fig. 4 to clarify the difference between panels i–l.
Q10:	All gene names should be set in italics, and protein names non-italic, please ensure all uses are consistent with this.

QUERY FORM

Nature Metabolism	
Manuscript ID	**[Art. Id: 467]**
Author	**Edward Milbank**

AUTHOR:

The following queries have arisen during the editing of your manuscript. Please answer by making the requisite corrections directly in the e.proofing tool rather than marking them up on the PDF. This will ensure that your corrections are incorporated accurately and that your paper is published as quickly as possible.

Query No.	*Nature of Query*
Q11:	Please add individual descriptions to the caption to Fig. 8 to clarify the difference between panels m–p.
Q12:	Please check that all funders have been appropriately acknowledged and that all grant numbers are correct.
Q13:	If applicable, please ensure accession codes are scheduled for release on or before this article's scheduled publication date, and update the database record with publication details from this article once available.
Q14:	Please check that the Competing Interests declaration is correct as stated. If you declare competing interests, please check the full text of the declaration for accuracy and completeness.

nature research

Corresponding author(s): Ramaroson Andriantsitohaina & Miguel López

Last updated by author(s): Aug 24, 2021

Reporting Summary

Nature Research wishes to improve the reproducibility of the work that we publish. This form provides structure for consistency and transparency in reporting. For further information on Nature Research policies, see Authors & Referees and the Editorial Policy Checklist.

Statistics

For all statistical analyses, confirm that the following items are present in the figure legend, table legend, main text, or Methods section.

n/a	Confirmed
☐	☒ The exact sample size (*n*) for each experimental group/condition, given as a discrete number and unit of measurement
☐	☒ A statement on whether measurements were taken from distinct samples or whether the same sample was measured repeatedly
☐	☒ The statistical test(s) used AND whether they are one- or two-sided *Only common tests should be described solely by name; describe more complex techniques in the Methods section.*
☐	☒ A description of all covariates tested
☒	☐ A description of any assumptions or corrections, such as tests of normality and adjustment for multiple comparisons
☐	☒ A full description of the statistical parameters including central tendency (e.g. means) or other basic estimates (e.g. regression coefficient) AND variation (e.g. standard deviation) or associated estimates of uncertainty (e.g. confidence intervals)
☐	☒ For null hypothesis testing, the test statistic (e.g. *F*, *t*, *r*) with confidence intervals, effect sizes, degrees of freedom and *P* value noted *Give P values as exact values whenever suitable.*
☒	☐ For Bayesian analysis, information on the choice of priors and Markov chain Monte Carlo settings
☒	☐ For hierarchical and complex designs, identification of the appropriate level for tests and full reporting of outcomes
☐	☒ Estimates of effect sizes (e.g. Cohen's *d*, Pearson's *r*), indicating how they were calculated

Our web collection on statistics for biologists contains articles on many of the points above.

Software and code

Policy information about availability of computer code

Data collection	ImageJ 1.44p; FLIR-Tools-Software Version 6.4; NTA Software Version 3.1; Multispectral imaging system MAESTRO Version 2.10.0; Fluorescence Imaging System Software Version 2.10.0; Bruker Albira Software Version 5.0; Leica Application Suite Advanced Fluorescence, Fiji, LAS X software Version 3.7.
Data analysis	Microsoft Excel 365; GraphPad Prism 8; GraphPad Instat 3.10; FLIR-Tools-Software Version 6.4; NTA Software Version 3.1; Multispectral imaging system MAESTRO Version 2.10.0; Fluorescence Imaging System Software Version 2.10.0; Bruker Albira Software Version 5.0; Leica Application Suite Advanced Fluorescence, Fiji, LAS X software Version 3.7; AMIDE Software 0.9.0.

For manuscripts utilizing custom algorithms or software that are central to the research but not yet described in published literature, software must be made available to editors/reviewers. We strongly encourage code deposition in a community repository (e.g. GitHub). See the Nature Research guidelines for submitting code & software for further information.

Data

Policy information about availability of data

All manuscripts must include a data availability statement. This statement should provide the following information, where applicable:

- Accession codes, unique identifiers, or web links for publicly available datasets
- A list of figures that have associated raw data
- A description of any restrictions on data availability

Source data files are provided with this article. All additional data that support the findings of this study are available from the corresponding authors (RA and ML) upon request.

Field-specific reporting

Please select the one below that is the best fit for your research. If you are not sure, read the appropriate sections before making your selection.

☒ Life sciences ☐ Behavioural & social sciences ☐ Ecological, evolutionary & environmental sciences

For a reference copy of the document with all sections, see nature.com/documents/nr-reporting-summary-flat.pdf

Life sciences study design

All studies must disclose on these points even when the disclosure is negative.

Sample size	For animal experiments, sample size was chosen based on similar previous studies of our group and based on literature documentation of similar well-characterized experiments. Statistical methods were not used to predetermine sample sizes. We try to use the fewest number of mice to achieve statistical significance without compromising the outcomes. The sample size is provided in figure legends and in the Statistical Analysis section in Methods.
Data exclusions	Samples of animals were excluded whether their values were outside the 2SD range. Criteria were pre-established.
Replication	All attempts to replicate the experiments have been successful. Experiments were repeated at least twice.
Randomization	Before starting an experiment, all mouse groups were made with set of animals of the same sex, age and similar body weight.
Blinding	For practical reasons, the investigators were not blinded to allocation during experiments and outcome assessment.

Reporting for specific materials, systems and methods

We require information from authors about some types of materials, experimental systems and methods used in many studies. Here, indicate whether each material, system or method listed is relevant to your study. If you are not sure if a list item applies to your research, read the appropriate section before selecting a response.

Materials & experimental systems

n/a	Involved in the study
☐	☒ Antibodies
☐	☒ Eukaryotic cell lines
☒	☐ Palaeontology
☐	☒ Animals and other organisms
☒	☐ Human research participants
☒	☐ Clinical data

Methods

n/a	Involved in the study
☒	☐ ChIP-seq
☒	☐ Flow cytometry
☐	☒ MRI-based neuroimaging

Antibodies

Antibodies used

* PRIMARY ANTIBODIES:
- Acetyl-CoA Carboxylase Antibody (1:1000, Cell Signaling Technology Cat# 3662, RRID:AB_2219400)
- AffiniPure Fab Fragment Goat Anti-Rabbit IgG (H+L) antibody (1:30, Jackson ImmunoResearch Labs Cat# 111-007-003, RRID:AB_2337925)
- Anti-GFAP antibody produced in goat (1:1000, Sigma-Aldrich Cat# SAB2500462, RRID:AB_10603437)
- Anti-GRP 94 Antibody (H-10) (1 :200, Santa Cruz Biotechnology Cat# sc-393402, Clone H-10,RRID:AB_2892568)
- Anti-UCP1 antibody (1:5000, Abcam Cat# ab10983, RRID:AB_2241462)
- Anti-UCP3 antibody (1:1000, Abcam Cat# ab3477, RRID:AB_2304253)
- CD9 (C-4) antibody (1:1000, Santa Cruz Biotechnology Cat# sc-13118, Clone C-4, RRID:AB_627213)
- CD81 (B-11) antibody (1:1000, Santa Cruz Biotechnology Cat# sc-166029, Clone B-11, RRID:AB_2275892)
- Iba1 Antibody (1:500, Novus Cat# NB 100-1028, RRID:AB_521594)
- LAMP2b antibody (1:1000, Abcam Cat# ab18529, RRID:AB_2134632)
- Monoclonal Anti-alpha-Tubulin antibody (1:5000, Sigma-Aldrich Cat# T5168, Clone B-5-1-2, RRID:AB_477579)
- Mouse Anti-beta-Actin Monoclonal Antibody (1:5000, Sigma-Aldrich Cat# A5316, Clone AC-74, RRID:AB_476743)
- Mouse Anti-Tsg 101 Monoclonal antibody (1:1000, Santa Cruz Biotechnology Cat# sc-7964, Clone C-2, RRID:AB_671392)
- PGC-1α Antibody (D-5) (1:1000, Santa Cruz Biotechnology Cat# sc-518025, Clone D-5, RRID:AB_2890187)
- PGC-1 beta (E-9) antibody (1:1000, Santa Cruz Biotechnology Cat# sc-373771, Clone E-9 RRID:AB_10915290)
- Phospho-Acetyl-CoA Carboxylase alpha (Ser79) Antibody (1:1000, Cell Signaling Technology Cat# 3661, RRID:AB_330337)
- Phospho-Acetyl-CoA Carboxylase alpha (Ser79) Polyclonal Antibody (1:50 and 1:100, Thermo Fisher Scientific Cat# PA5-17725, RRID:AB_10981245)
- Purified anti-Alix antibody (1:1000, Biolegend, Cat# 634502, Clone 3A9, RRID:AB_2162471)
- Steroidogenic Factor 1 antibody (1:200, Abcam Cat# ab65815, RRID:AB_1925469)

* SECONDARY ANTIBODIES:
- Alexa Fluor® 594 AffiniPure Donkey Anti-Rabbit IgG (H+L) antibody (1:1000, Jackson ImmunoResearch Labs Cat# 711-585-152, RRID:AB_2340621)
- Donkey anti-Goat IgG (H+L) Cross-Adsorbed Secondary Antibody, Alexa Fluor 488 (1:1000, Thermo Fisher Scientific Cat# A-11055, RRID:AB_2534102)
- Donkey anti-Rabbit IgG (H+L) Highly Cross-Adsorbed Secondary Antibody, Alexa Fluor 594 (1:1000, Thermo Fisher Scientific Cat# A-21207, RRID:AB_141637)
- Donkey anti-Rabbit IgG (H+L) Highly Cross-Adsorbed Secondary Antibody, Alexa Fluor 647 (1:1000, Thermo Fisher Scientific Cat# A-31573, RRID:AB_2536183)
- Goat Anti-Rabbit Immunoglobulins/HRP antibody (1:5000, Agilent Cat# P0448, RRID:AB_2617138)
- Rabbit Anti-Mouse Immunoglobulins/HRP antibody (1:5000, Agilent Cat# P0260, RRID:AB_2636929)

Validation

All antibodies used in this paper have been validated by the manufacturer (associated datasheet for each referenced antibody), by our former papers or in the literature (all articles using one of the listed antibodies can be found on the RRID portal https://scicrunch.org/resources).

Eukaryotic cell lines

Policy information about cell lines

Cell line source(s)

- The JAWS II dendritic cell line was purchased from the American Type Culture Collection (ATCC, CRL-1194)
- The mouse hypothalamic GT1-7 cell line was gently provided by Eduardo Domínguez and Prof Mabel Lóza (University of Santiago de Compostela, Spain)
- The mouse neuroblastoma Neuro-2A cell line was generously provided by the laboratory Micro et Nanomédecines Translationnelles (University of Angers, France)
- Immortalized brown adipocytes from C57BL/6J mice were obtained from Francesc Villarroya's laboratory (PMID: 31411815)
- The U2OS (WT and AMPK KO) cell lines were obtained from Reuben Shaw's laboratory (Molecular and Cell Biology Laboratory and Howard Hughes Medical Institute, Salk Institute for Biological Studies, La Jolla, CA 92037, USA) (PMID: 26816379)

Authentication

None of the cell lines described above were authenticated

Mycoplasma contamination

All cell lines were tested negative for mycoplasma contamination

Commonly misidentified lines
(See ICLAC register)

n/a

Animals and other organisms

Policy information about studies involving animals; ARRIVE guidelines recommended for reporting animal research

Laboratory animals

C57BL/6 mice (8-12 weeks; male; 25g; Centro de Biomedicina Experimental; Santiago de Compostela, Spain or Jackson Laboratory, USA), nude mice (8-12 weeks; male; NRj:NMRI-Foxn1nu/Foxn1nu; Janvier Labs; Saint Berthevin, France) and C57BL/6 homozygous UCP1 knockout (8-12 weeks; male; UCP1-KO; ucp1-/-) males and their corresponding wild-type littermates50 (bred in the GTH University of Lübeck, Germany) were used for the experiments. Animals were housed with an artificial 12-h light (8:00 to 20:00)/12-h dark cycle, under controlled temperature and humidity conditions and allowed to free access to regular chow diet or 60% HFD (D12492; Research Diets, Inc; New Brunswick, USA) and filtered tap water for 10 weeks. For all the procedures, the animals were caged individually, and became accustomed to the handling procedure under non-stressful conditions.

Wild animals

This study did not involve wild animals

Field-collected samples

This study did not involve field-collected samples

Ethics oversight

The experiments were performed in agreement with the International Law on Animal Experimentation and were approved by the USC Ethical Committee (Project ID 15010/14/006 and 15012/2020/010), the University of Iowa Animal Research Committee (Protocol 8101549) and MELUR Schleswig Holstein (77/7-19).

Note that full information on the approval of the study protocol must also be provided in the manuscript.

Magnetic resonance imaging

Experimental design

Design type

MRI studies were performed in 2 groups of adult (8-12 weeks) male mice: control and treated (n=8 animals/group).

Design specifications

One MRI study was performed per animal with the following sequences: 1. Localizer; 2. Flash; 3 Flash
Total acquisition time was 31 minutes.
NMR procedures were carried out under sevoflurane anesthesia (6% induction and 3.5% maintenance in a gas mixture of 70% NO2 and 30% O2).

All studies were conducted on a 9.4T horizontal bore magnet (Bruker BioSpin, Ettlingen, Germany) with 440 mT/m gradients.

Behavioral performance measures: n/a

Acquisition

Imaging type(s): Structural sequences

Field strength: 9.4 Tesla

Sequence & imaging parameters: FLASH sequences with repetition time/echo time (RT/ET) = 1300/3.5 ms, number of averages (NA)= 2, 30 coronal slices of 1 mm, field of view (FOV) = 60×80 mm and matrix size = 256×350 (in plane resolution of 0.234 x 0.229 mm/pixel) were acquired with and without fat suppression option to generate both "fat-suppression" and "fat" image sets. Total acquisition time was 31 minutes.

Area of acquisition: Semi-automatic image processing was used to create fat brain masks comparing co-registered image sets with and without fat suppression option.

Diffusion MRI ☐ Used ☒ Not used

Preprocessing

Preprocessing software: The MR post-processing was performed using ImageJ software (W. Rasband, NIH, USA).

Normalization: Data were not normalized.
Semi-automatic image processing was used to create fat masks (volumes of total (Total AT), subcutaneous adipose tissue (scAT) and visceral adipose tissue (vAT)) comparing co-registered image sets with and without fat suppression option. Using a standard density for adipose tissue (0.9 g/ml) and other tissues (1.04 g/ml), we converted the MRI volumes to weights.

Normalization template: Data were not normalized.

Noise and artifact removal: Motion suppression option was selected in the sequence parameters. Images were co-registered for further processing.

Volume censoring: ImageJ software. Brain regions were segmented semi-automatically. Using a standard density for adipose tissue (0.9 g/ml) and other tissues (1.04 g/ml); MRI volumes were converted to weights.

Statistical modeling & inference

Model type and settings: From co-registered image sets with and without fat suppression option and using a standard density for adipose tissue (0.9 g/ml) and other tissues (1.04 g/ml); MRI volumes were converted to weights. Data were expressed as mean±SEM.

Effect(s) tested: n/a

Specify type of analysis: ☐ Whole brain ☒ ROI-based ☐ Both

Anatomical location(s): Semi-automatic image processing was used to create fat masks (volumes of total (Total AT), subcutaneous adipose tissue (scAT) and visceral adipose tissue (vAT)) comparing co-registered image sets with and without fat suppression option. Using a standard density for adipose tissue (0.9 g/ml) and other tissues (1.04 g/ml); MRI volumes were converted to weights.

Statistic type for inference (See Eklund et al. 2016): n/a

Correction: n/a

Models & analysis

n/a	Involved in the study
☒	☐ Functional and/or effective connectivity
☐	☒ Graph analysis
☒	☐ Multivariate modeling or predictive analysis

Graph analysis: From co-registered image sets with and without fat suppression option and using a standard density for adipose tissue (0.9 g/ml) and other tissues (1.04 g/ml); MRI volumes were converted to weights.